

Accepted for publication in ApJ.

X-Ray Synchrotron Emission from 10–100 TeV Cosmic-Ray Electrons in the Supernova Remnant SN 1006

G. E. Allen

*MIT Center for Space Research, 77 Massachusetts Avenue, NE80-6029, Cambridge, MA
02139-4307*

R. Petre

*NASA/Goddard Space Flight Center, Laboratory for High Energy Astrophysics, Code 662,
Greenbelt, MD 20771*

and

E. V. Gotthelf

*Columbia Astrophysics Laboratory, Columbia University, Pupin Hall, 550 West 120th Street, New
York, NY 10027*

ABSTRACT

We present the results of a joint spectral analysis of *RXTE* PCA, *ASCA* SIS, and *ROSAT* PSPC data of the supernova remnant SN 1006. This work represents the first attempt to model both the thermal and nonthermal X-ray emission over the entire X-ray energy band. The thermal flux is described by a nonequilibrium ionization model with an electron temperature $kT_e = 0.6$ keV, an ionization timescale $n_0 t = 9 \times 10^9 \text{ cm}^{-3} \text{ s}$, and a relative elemental abundance of silicon that is 10–18 times larger than the solar abundance. The nonthermal X-ray spectrum is described by a broken power law model with low- and high-energy photon indices $\Gamma_1 = 2.1$ and $\Gamma_2 = 3.0$, respectively. Since the nonthermal X-ray spectrum steepens with increasing energy, the results of the present analysis corroborate previous claims that the nonthermal X-ray emission is produced by synchrotron radiation. We argue that the magnetic field strength is significantly larger than previous estimates of about $10 \mu\text{G}$ and arbitrarily use a value of $40 \mu\text{G}$ to estimate the parameters of the cosmic-ray electron, proton, and helium spectra of the remnant. The results for the ratio of the number densities of protons and electrons ($R = 160$ at 1 GeV), the total energy in cosmic rays ($E_{\text{cr}} = 1 \times 10^{50}$ ergs), and the spectral index of the electrons at 1 GeV ($\Gamma_e = 2.14 \pm 0.12$) are consistent with the hypothesis that Galactic cosmic rays are accelerated predominantly in the shocks of supernova remnants. Yet, the remnant may or may not accelerate nuclei to energies as high as the energy of the “knee,” depending on the reason why the maximum energy of the electrons is only 10 TeV.

Subject headings: acceleration of particles — cosmic rays — ISM: individual (SN 1006)
— radiation mechanisms: nonthermal — supernova remnants — X-rays: general

1. Introduction

The search for evidence of the origin of Galactic cosmic rays has been an active area of research for many decades. While little evidence exists about the sites at which very high energy nuclei are accelerated, the results of recent X-ray and gamma-ray observations indicate that at least some of the cosmic-ray electrons are accelerated in the shocks of supernova remnants (Koyama et al. 1995, 1997; Allen et al. 1997; Tanimori et al. 1998; Allen, Gotthelf, & Petre 1999; Vink et al. 1999; Slane et al. 1999; Muraishi et al. 2000; Borkowski et al. 2000; Dyer et al. 2001a). For example, SN 1006 is one remnant for which there is evidence that cosmic-ray electrons have been accelerated to energies as high as about 100 TeV (Koyama et al. 1995; Tanimori et al. 1998). In this paper, measurements of the X-ray and radio emission of the remnant are used to determine the parameters of the nonthermal electron spectrum. Although there is no evidence to indicate that cosmic-ray nuclei are accelerated in SN 1006, relativistic electrons and nuclei are expected to be accelerated in a similar manner (Ellison & Reynolds 1991). Therefore, we estimate the parameters of the proton and helium spectra of the remnant. The results of this analysis show that the remnant is a significant source of Galactic cosmic rays (at least cosmic-ray electrons) and provide some support for the idea that Galactic cosmic rays are accelerated predominantly in the shocks of supernova remnants.

Section 2 contains a description of some of the results of previous analyses of the X-ray data of SN 1006. The data and analysis techniques used for the present work are described in section 3. Section 4 includes a discussion of the results of the present analysis. The conclusions are reviewed in section 5.

2. Observational X-Ray Record

The first detection of X-ray emission from SN 1006 was reported by Winkler & Laird (1976). The results of analyses of X-ray spectral data of the remnant have been reported by many authors (Winkler & Laird 1976; Zarnecki & Bibbo 1979; Winkler et al. 1979; Toor 1980; Becker et al. 1980; Pye et al. 1981; Galas, Venkatesan, & Garmire 1982; Vartanian, Lum, & Ku 1985; Hamilton, Sarazin, & Szymkowiak 1986; Koyama et al. 1987, 1995; Leahy, Nousek, & Hamilton 1991; Ozaki et al. 1994; Willingale et al. 1996; Reynolds 1996; Laming 1998; Vink et al. 2000; Dyer et al. 2001a). As early as 1979, it was realized that the global X-ray spectrum of SN 1006 cannot be fitted with a single thermal or nonthermal model (Winkler et al. 1979). This realization is not surprising in retrospect because observations of the remnant with imaging X-ray devices show that the X-ray spectrum varies as a function of position in the remnant. The high-energy X-ray image of the

remnant, like the radio image, is dominated by emission from the northeastern and southwestern rims (Pye et al. 1981; Willingale et al. 1996; Winkler & Long 1997). Since the spectra of the rims are more or less featureless, the emission from these regions is reported to be nonthermal (Koyama et al. 1995; Reynolds 1996; Dyer et al. 2001a). At energies of less than 0.5 keV, a significant amount of emission is observed from the interior of the remnant, especially in the southwest (Pye et al. 1981; Willingale et al. 1996). Since the X-ray spectrum of the interior exhibits atomic emission-line features, a substantial amount of the emission from this region must be thermal bremsstrahlung.

Several of the spectral analyses of SN 1006 included two spectral components. Invariably, one of the spectral components is thermal emission from an optically thin plasma. Such a model is needed to describe the emission-line features of oxygen, neon, magnesium, silicon, and perhaps iron (Koyama et al. 1995; Vink et al. 2000; Dyer et al. 2001a). Some analyses have included an additional thermal component, while others have included a nonthermal component. For example, Hamilton et al. (1986) modeled the spectrum using two thermal components. One component is used to describe the forward-shocked interstellar medium, and the other describes the reverse-shocked ejecta. To explain the nearly featureless nature of the global X-ray spectrum of the remnant, they used a model for the shocked ejecta in which most of the emission is produced by a nearly pure layer of fully ionized carbon. The elements more massive than carbon are assumed to be significantly underionized in the ejecta, to suppress the X-ray line emission that would otherwise be produced by these elements. However, these assumptions are inconsistent with the results of subsequent analyses. The results of an analysis of the ultraviolet absorption-line features along the line of sight to the S-M star suggest that most of the ejected silicon has already been shocked (Hamilton et al. 1997), and therefore may not be in a low ionization state. This result is supported by X-ray observations that reveal line emission from several highly ionized elements: oxygen, neon, magnesium, silicon, and perhaps iron (Koyama et al. 1995; Vink et al. 2000; Dyer et al. 2001a). Since the relative abundance of the shocked silicon producing the X-ray emission is much larger than the relative abundance of silicon in the solar system, most of the shocked silicon is ejecta. Furthermore, the results of the analysis of Laming (1998) suggest that the total amount of reverse-shocked carbon required by the model of Hamilton et al. may be unreasonably large for the remnant of a type Ia supernova (i.e., may be well in excess of the Chandrasekhar mass). For these reasons, the thermal model of Hamilton et al. provides a poor description of the X-ray emission of SN 1006.

Willingale et al. (1996) present a nonthermal interpretation of the high-energy X-ray emission. They argue that the X-ray emission from the rims is produced by relativistic electrons that are beamed from an unobserved central compact object. This conclusion seems to be based largely on the X-ray morphology of SN 1006, because no evidence of a compact object or of particle jets in the remnant has been reported. For comparison, the pulsar and the pulsar jet of the Vela supernova remnant are observed to produce radio, X-ray, and gamma-ray emission (Markwardt & Ögelman 1995; Yoshikoshi et al. 1997; Bock, Turtle, & Green 1998). Willingale et al. (1996) set an upper limit on the flux of a point source of 6.3×10^{-14} erg cm $^{-2}$ s $^{-1}$. The corresponding constraint on the blackbody temperature of a 10 km neutron star is $T_{\text{BB}} < 6.9 \times 10^5$ K (at a distance of 1.7 kpc).

Some of the models of cooling neutron stars indicate that the temperature of a neutron star is higher than this upper limit at an age of 990 yr (Slane & Lloyd 1995). Furthermore, the sketchy record of the optical light curve of the supernova (Schaefer 1996), the lack of evidence of an OB association near SN 1006 (Hamilton et al. 1986), the large distance of the remnant from the plane of the Galaxy [$z = +430(d/1.7 \text{ kpc}) \text{ pc}$], measurements of the average expansion rate of the remnant (Moffett, Goss, & Reynolds 1993), and measurements of the relative abundances of the elements producing the ultraviolet absorption lines (Fesen et al. 1988) suggest that SN 1006 was produced by a type Ia supernova. Type Ia supernovae are generally not expected to produce compact objects. For these reasons, it seems unlikely that SN 1006 contains an undetected compact object that is responsible for the high-energy X-ray emission from the rims.

Koyama et al. (1995) advance an alternative nonthermal explanation of the high-energy X-ray emission. They conclude that the emission from the rims is synchrotron radiation from electrons that have been accelerated to energies of about 100 TeV. Reynolds (1996) argues convincingly that this conclusion is the only plausible one and shows that the nonthermal X-ray emission of the rims can be described by a model in which both the radio and X-ray emission are produced by a common population of shock-accelerated electrons. The strong correlation of the features of a high-energy X-ray image and a radio image of the northeastern rim of SN 1006 (Winkler & Long 1997) supports this result. Furthermore, the detection of inverse-Compton TeV gamma-ray emission from the northeastern rim of the remnant confirms the presence of very high energy electrons in SN 1006 (Tanimori et al. 1998). Since the TeV photons are produced by electrons that have energies similar to the energies needed to produce X-ray synchrotron radiation and since the radio, X-ray, and gamma-ray spectral data can be fitted with simple models of the spectrum of shock-accelerated electrons (Mastichiadis & de Jager 1996; Aharonian & Atoyan 1999), the conclusion that the nonthermal X-ray emission is produced by synchrotron radiation seems unavoidable.

3. Data and Analysis

To accurately model the shape of the entire X-ray spectrum of SN 1006, from 0.12 to 17 keV, we analyzed data obtained using the Proportional Counter Array (PCA) of the *Rossi X-Ray Timing Explorer* (*RXTE*) satellite, the Solid-state Imaging Spectrometers (SISs) of the *Advanced Satellite for Cosmology and Astrophysics* (*ASCA*), and the Position Sensitive Proportional Counter (PSPCB, hereafter just PSPC) of the *Röntgen* satellite (*ROSAT*). Between 1996 February 18 and 1996 February 20, SN 1006 was observed for 21 ks at a location on the northeastern rim ($\alpha_{2000} = 15^{\text{h}}4^{\text{m}}0$, $\delta_{2000} = -41^{\circ}48'$) and for 20 ks at a location on the southwestern rim ($\alpha_{2000} = 15^{\text{h}}1^{\text{m}}8$, $\delta_{2000} = -42^{\circ}6'$) using the PCA. The PCA is a spectrophotometer that is comprised of an array of five coaligned proportional counter units that are mechanically collimated to have a field of view of 1° FWHM (Jahoda et al. 1996). The array is sensitive to photons that have energies between about 2 and 60 keV and has an energy resolution $\Delta E/E = 0.18$ at 6 keV. The maximum on-axis collecting area is about 7000 cm^2 . The PCA data were screened to remove the time intervals

during which (1) one or more of the five proportional counter units is off, (2) SN 1006 is less than 10° above the limb of the Earth, (3) the background model is not well defined, and (4) the pointing direction of the detectors is more than $0^\circ.02$ from the nominal pointing direction in either right ascension or declination. The set of X-ray events that satisfies these four selection criteria includes 7 ks of the data of the northeastern pointing and 11 ks of the data of the southwestern pointing. Spectra were constructed for each of the two PCA pointings. The two spectra are quite similar because the field of view of the PCA is large enough to include the entire remnant at both pointing locations. Therefore, the PCA data are insensitive to modest changes in the shape of the spectrum of the remnant as a function of position in the remnant. The PCA background spectrum for SN 1006 was estimated using version 1.5 of the FTOOL *pcabackest*¹. This version of *pcabackest* includes an estimate of the charged-particle and diffuse cosmic X-ray backgrounds based on the “VLE” count rate during observations of “source-free” regions of the sky and an estimate of the background associated with the decay of radioactive material that is activated when the spacecraft passes through the South Atlantic Anomaly. The tool has been found to produce slightly inaccurate estimates of the background associated with astrophysical sources. For example, when the background spectrum is subtracted from the spectral data of SN 1006, the resulting “source” spectrum of the remnant has a negative count rate at high energies. To compensate for this problem, the spectrum of the background associated with the South Atlantic Anomaly is multiplied by a factor of 0.2. This factor is determined by requiring the average difference between the source spectrum and the source model to be zero at energies between 27 and 71 keV. In this energy band, the total number of events associated with SN 1006 is expected to be negligibly small compared to the number of events associated with the background. The adjustment reduces the count rate of the 2–10 keV activation background from 1.0 to 0.2 counts s^{-1} for the top layer of anodes in the PCA. After applying this adjustment, the average 2–10 keV background count-rate for the top layer is estimated to be 17.2 ± 0.1 counts s^{-1} for both pointings.

On 1993 August 19–20, 1993 September 13–15, and 1996 February 20–21, the instruments on ASCA (Tanaka, Inoue, & Holt 1994) were used to observe SN 1006 for 43 ks at a location in the center of the remnant ($\alpha_{2000} = 15^{\text{h}}2^{\text{m}}48^{\text{s}}$, $\delta_{2000} = -41^\circ55'46''$), for 38 ks at a location on the northeastern rim ($\alpha_{2000} = 15^{\text{h}}3^{\text{m}}32^{\text{s}}$, $\delta_{2000} = -41^\circ46'25''$), and for 57 ks at a location on the southwestern rim ($\alpha_{2000} = 15^{\text{h}}2^{\text{m}}34^{\text{s}}$, $\delta_{2000} = -42^\circ2'58''$), respectively. The SIS detectors are CCD devices (Burke et al. 1994) sensitive to photons that have energies between about 0.5 and 10 keV. The devices have an energy resolution $\Delta E/E = 0.06$ – 0.08 (FWHM) at 1.5 keV and a field of view of $22' \times 22'$. The spatial resolution of the telescope $\lesssim 1.5'$ (50% encircled-photon radius) for the SIS data used here. The maximum on-axis effective area of the system is about 220 cm^2 . The SIS data were screened using the standard “REV2” criteria that exclude time intervals (1) associated with passages through the South Atlantic Anomaly and regions of relatively high particles fluxes, (2) during which the bright limb of the Earth is in the field of view, and (3) during which the source is occulted by the Earth. The set of X-ray events that satisfies these selection criteria includes 23,

¹For more information about FTOOLS, see http://heasarc.gsfc.nasa.gov/docs/software/ftools/ftools_menu.html.

20, and 43 ks of data for the center, northeastern rim, and southwestern rim, respectively. The SIS spectra for these three spatially separate regions, which correspond to the central, northeastern, and southwestern ovals of Figure 1, have event rates of 0.21, 0.89, and 0.66 counts s⁻¹, respectively.

On 1993 January 28–29, SN 1006 was observed for 6 ks at a location near the center of the remnant ($\alpha_{2000} = 15^{\text{h}}2^{\text{m}}55^{\text{s}}$, $\delta_{2000} = -41^{\circ}55'12''$) using the PSPC. The PSPC is a multiple-wire proportional counter sensitive to photons that have energies between about 0.1 and 2 keV. The energy resolution $\Delta E/E = 0.43$ at 0.93 keV. The telescope has a field of view of 2° . The spatial resolution $\lesssim 30''$ (50% encircled-photon radius) for the PSPC data used here. The maximum on-axis effective area of the system is about 260 cm² (Pfeffermann et al. 1987). Spectra were constructed using the PSPC data for three spatially separate regions: the bright northeastern rim, the bright southwestern rim, and the center of the remnant (the three rectangular regions of Fig. 1). The total PSPC event rates for these three spectra are 5.6, 6.1, and 11.9 counts s⁻¹, respectively. The PSPC background for SN 1006 is negligibly small. Plucinsky et al. (1993) report that the event rate associated with unrejected cosmic-ray particles is 4×10^{-6} counts s⁻¹ keV⁻¹ arcmin⁻² in the pulse-height range $18 \leq \text{PHA} \leq 249$. In this case, the cosmic-ray event rate over the entire remnant is only about 3×10^{-3} counts s⁻¹ keV⁻¹. Since this rate is considerably smaller than the PSPC count-rate for SN 1006 at all energies from 0.12 to 2 keV, the background is neglected.

A joint fit to the *RXTE* PCA, *ASCA* SIS, and *ROSAT* PSPC data was performed using version 10.0 of the spectral-fitting software package XSPEC². Since Koyama et al. (1995) and others report evidence of both thermal and nonthermal emission, the spectral fits were performed using several combinations of thermal and nonthermal emission components. The thermal components include a bremsstrahlung model (Brem), a model of a thin thermal plasma in collisional ionization equilibrium (RS; Raymond & Smith 1977), and a model of a thin thermal plasma that is not in ionization equilibrium (NEI; Hamilton, Sarazin, & Chevalier 1983). The nonthermal components include power law (PL) and broken power law (BPL) models. For each fit, only the absolute normalization of each spectral component was allowed to vary from one region to another. While the spectra most likely vary as a function of position in the remnant, we find no evidence of a significant variation in the shape of the nonthermal spectra of the different regions. Furthermore, Koyama et al. (1995) and Vink et al. (2000) report no evidence of spatial variation in the emission of the interior of the remnant.

Table 1 summarizes the results of some of the fits. Note that the values of $\chi^2/\nu > 1$ for all of the fits. This result suggests that the value of χ^2 may be sensitive to systematic errors in the responses of the detectors as well as differences between the spectral models and the spectral data. Therefore, the χ^2 test statistic does not provide an unambiguous measure of the goodness of fit of the models. However, if the contributions of the systematic errors to χ^2 do not change from one fit to another, the differences in χ^2 provide a useful measure of the relative goodness of fit of the different models. In this case, $\Delta\chi^2 = \chi^2 - \chi_{\text{min}}^2$ is distributed as a χ^2 variable with the number of

²For more information about XSPEC, see <http://heasarc.gsfc.nasa.gov/docs/xanadu/xspec/index.html>.

degrees of freedom equal to the number of free parameters in the fit (Lampton, Margon, & Bowyer 1976). For example, 26 free parameters are used for the best-fit model of Table 1. Therefore, the values of $\Delta\chi^2 = 28.9, 35.6, 39.3$, and 50.6 are expected to correspond to the 1σ , 90%, 2σ , and 3σ confidence levels, respectively. These values of $\Delta\chi^2$ are used in this paper to determine the confidence intervals of the fit and inferred parameters. Since the differences between the value of χ^2 for the BPL+NEI model and the values of χ^2 for the other sets of models ≥ 93 , the BPL+NEI model seems to provide a significantly better fit to the entire broadband spectral data than the other sets of models listed in Table 1. Table 2 lists the fit parameters of the BPL+NEI model. The spectral data and the best-fit model are shown in Figures 2–4. In general, the model fits the 0.12–17 keV data quite well.

The thermal component of the best-fit model is a nonequilibrium ionization model of a thin thermal plasma that has different electron and ion temperatures (Hamilton et al. 1983). The shape of the X-ray continuum is specified by the temperature associated with the forward shock, T_{fs} , and the parameter $n_0^2 E_0$, where n_0 is the ambient density of interstellar hydrogen and E_0 is the initial kinetic energy of the ejecta. This model is implemented in XSPEC version 10.0 using a fixed grid in the $T_{\text{fs}}-n_0^2 E_0$ plane. The temperature is quantized by factors of $10^{0.25}$ from $10^{6.25}$ to $10^{8.25}$ K and $n_0^2 E_0$ is quantized by factors of 10 from 10^{48} to 10^{53} ergs cm $^{-6}$. The best-fit values of these two parameters are $T_{\text{fs}} = 10^{8.0}$ K and $n_0^2 E_0 = 10^{50}$ ergs cm $^{-6}$ (Fig. 5). Figure 5 includes curves along which the ionization timescale, $n_0 t$, and the characteristic electron temperature, kT_e , are constant. The elongated confidence level contours in this figure nearly lie along curves of constant ionization timescale. The best-fit values of T_{fs} and $n_0^2 E_0$ are driven by the thermal emission of SN 1006 because the same values for these two parameters (within the statistical uncertainties) are obtained if the same set of spectral models is fitted to only the *ASCA* SIS spectrum of the center of the remnant. The relative elemental abundances of the elements oxygen, neon, magnesium, and silicon are included as free parameters in the fit because the *ASCA* SIS spectrum of the central region of SN 1006 exhibits atomic emission-line features associated with these elements (Koyama et al. 1995). The abundances of sulphur and calcium are fixed to be the same as the abundance of silicon because this situation is more or less consistent with the type Ia supernova model of Nomoto, Thielemann, & Yokoi (1984). Since the value of χ^2 is not significantly reduced if the abundances of helium, carbon, nitrogen, iron, or nickel are included as free parameters in the fit, these five abundances are set to be the same as the relative abundances of these elements in the solar system (Anders & Grevesse 1989). The fitted abundances of oxygen and magnesium are consistent with the solar abundances of these elements. The abundance of neon in SN 1006 is less than 80% of the relative solar abundance of neon. The fitted relative abundance of silicon (and sulphur and calcium) is 10–18 times larger than the solar abundance of silicon. The uncertainties of the abundances are somewhat larger than the statistical uncertainties specified in Table 2 because (Hamilton et al. 1983) note that the intensities used in the NEI model for the strong emission lines are generally uncertain by at least a factor of 2.

A broken power law model is used here to approximate a gradually steepening nonthermal X-

ray spectrum. Such a spectrum is expected if the nonthermal emission is produced by synchrotron radiation (Reynolds 1996). As shown in Figure 6, the nonthermal spectrum of SN 1006 steepens significantly with increasing energy. The difference between the high-energy and low-energy photon indices of the broken power law ≥ 0.7 at the 3σ confidence level. The value of the break energy of the broken power law ($E_b = 1.85 \pm 0.18$ keV) is not physically meaningful. It does not correspond to a feature in the nonthermal X-ray spectrum of SN 1006. This value is determined by the transition from the relatively high count rate portion of the *ROSAT* PSPC spectrum to the relatively high count rate portion of the *RXTE* PCA spectrum.

4. Discussion

4.1. Thermal Emission

Only one thermal emission model is used in the present analysis to describe the properties of the X-ray-emitting material in SN 1006. The use of one thermal component is undoubtedly an oversimplification, because both the forward-shocked interstellar material and the reverse-shocked ejecta produce X rays. The large fitted abundance of silicon suggests that most of the shocked silicon is ejecta. Yet the inferred amount of swept-up mass implies that most of the shocked mass is interstellar. For these reasons, the use of a single thermal model to describe the global thermal emission properties of the remnant may provide a poor description of any given volume element of the X-ray-emitting material. Nevertheless, the use of a single thermal model is sufficient to accurately characterize the properties of the nonthermal X-ray emission (our primary goal), because the X-ray emission of the remnant is dominated by nonthermal emission at energies above 1 keV, because the results for the broken power law component are insensitive to the details of the single thermal component used in the fits (compare the results obtained for the broken power laws of the “BPL+NEI” and “BPL+RS” models listed in Table 1), and because Koyama et al. (1995) and Vink et al. (2000) report no evidence of spatial variation of the thermal X-ray spectrum of the interior of SN 1006.

Models that include two thermal components and one nonthermal component were fitted to the data. However, the results for the fit parameters of these three-component models showed that the parameters of one of the two thermal components are essentially unconstrained.

Vink et al. (2000) favor a model for the X-ray emission of the interior of SN 1006 that includes two thermal components instead of one thermal component and one nonthermal component. They find that the temperatures of the hotter thermal components $kT_e > 3$ keV for both the northern and southern regions of the interior. These temperatures are quite high for the observed Galactic supernova remnants. Of the young, shell-type remnants, only Cassiopeia A is reported to have a thermal plasma with a temperature this high. Hamilton & Sarazin (1984) show that it may be possible for a reverse-shocked silicon-dominated plasma to have electron temperatures this high, but such a metal-rich plasma would cool quickly. Therefore, the cooling time would have to be

comparable to the age of the remnant or longer. Otherwise, the reverse-shocked electrons may be too cool to produce much X-ray emission. The model of Vink et al. (2000) cannot explain nonthermal X-ray emission from the interior of the remnant. Since Dyer et al. (2001b) show that about 25% of the radio emission at 843 MHz is produced in the interior of SN 1006, a similar fraction of nonthermal X-ray synchrotron emission is expected from this region. Our fits to the X-ray data with a model that includes one thermal and one nonthermal component suggest that $13 \pm 7\%$ of the nonthermal X-ray emission is produced in the region. Since this fraction is comparable to the fraction of the radio emission from the interior of SN 1006, we favor a model for the interior (and the rims) that includes one thermal component and one nonthermal component instead of two thermal components. It should be emphasized that the principal results of the present analysis concerning the properties of the cosmic rays in SN 1006 are insensitive to this choice, since only a small fraction of the high-energy X-ray emission is produced in the interior of the remnant.

The parameters of the best-fit model are listed in Table 2. Table 3 includes a list of the inferred values of the characteristic energy of the thermal electrons, kT_e (see Fig. 5), the velocity of the forward shock, v_{fs} , the radius of the forward shock, r_{fs} , the distance of the remnant, d , the ionization timescale, $n_0 t$ (see Fig. 5), the age of the remnant, t , the density of interstellar hydrogen, n_0 , and the swept-up mass, M_s (Hamilton et al. 1983). These inferences are based on the assumptions that SN 1006 is in a Sedov phase, that the initial kinetic energy of the ejecta is 10^{51} ergs, that the X-ray emission is dominated by forward-shocked interstellar material, and that the distribution of the ambient material around SN 1006 is homogeneous.

The best-fit value for the absorption column density of interstellar hydrogen $n_H = (5.6 \pm 0.6) \times 10^{20}$ atoms cm^{-2} (at the 90% confidence level). This value is consistent with the result of Schaefer (1996) [$n_H = (6.1 \pm 0.6) \times 10^{20}$ atoms cm^{-2}], who analyzed a compilation of results from several sources. The relative elemental abundances of oxygen, neon, magnesium, and silicon are consistent with the results of Koyama et al. (1995), but Vink et al. (2000) obtain a somewhat lower abundance for oxygen. The inferred energy of the thermal electrons ($kT_e = 0.58_{-0.27}^{+0.02}$ keV at the 90% confidence level) is similar to the results obtained by Vink et al. (2000; $kT_e = 0.71 \pm 0.15$ and 0.78 ± 0.09 keV) and Dyer et al. (2001a; $kT_e = 0.60_{-0.52}^{+0.70}$), but it is somewhat lower than the result of Koyama et al. (1995; $kT_e = 1.6$ keV). The results of an analysis of the ultraviolet emission-line data of the northwestern rim favor a low electron temperature ($kT_e < 0.05kT_p = 0.05 \frac{3}{16} m_p v_{fs}^2 = 0.7$ keV), but the results cannot exclude temperatures as high as $kT_e = 2.9$ keV (Laming et al. 1996). The inferred shock velocity ($v_{fs} = 2700_{-1700}^{+200}$ km s^{-1} at the 90% confidence level) is consistent with the results of Kirshner, Winkler, & Chevalier (1987; $v_{fs} = 2800\text{--}3870$ km s^{-1}), Raymond, Blair, & Long (1995; $v_{fs} = 2300$ km s^{-1}), and Laming et al. (1996; $v_{fs} = 2600 \pm 300$ km s^{-1}) for the northwestern rim of SN 1006, but Dwarkadas & Chevalier (1998) argue that the average forward shock velocity is 4000 ± 500 km s^{-1} .

The inferred distance ($d = 1.4_{-0.1}^{+2.3}$ kpc at the 90% confidence level) is consistent with the result of Schaefer (1996; $d = 1.59 \pm 0.13$ kpc) and with a distance estimate that is based on the velocity and proper motion of the forward shock in the northwest. As described above, Laming et al.

(1996) estimate that the velocity of the forward shock in the northwest $v_{\text{fs}} = 2600 \pm 300 \text{ km s}^{-1}$. Since neutral atoms have very short lifetimes after having passed through the shock into the hot postshock gas, the $\text{H}\alpha$ filaments trace the location of the forward shock (Chevalier & Raymond 1978; Long, Blair, & van den Bergh 1988; Winkler & Long 1997). The results of analyses of the mean proper motion of the filaments along the northwestern rim of SN 1006 suggest that $\bar{\mu} = 0''.30 \pm 0''.04 \text{ yr}^{-1}$ (Long et al. 1988) or $\bar{\mu} = 0''.39 \pm 0''.06 \text{ yr}^{-1}$ (Hesser & van den Bergh 1981). The weighted average of these two results is $0''.33 \pm 0''.03 \text{ yr}^{-1}$. Therefore the implied distance of SN 1006 $d = v_{\text{fs}}/\langle\bar{\mu}\rangle = 1.66 \pm 0.24 \text{ kpc}$. These distance estimates are consistent with the upper and lower limits on the distance (Hamilton et al. 1986, 1997; Wu et al. 1993; Burleigh et al. 2000). Collectively, the results suggest that $1.4 \leq d \leq 2.0 \text{ kpc}$.

The ionization timescale ($n_0 t = 240\text{--}650 \text{ cm}^{-3} \text{ yr}$), age ($t = 760\text{--}6300 \text{ yr}$), and ambient density of interstellar hydrogen ($n_0 = 0.10\text{--}0.37 \text{ cm}^{-3}$), are consistent with the ionization timescale of Koyama et al. (1995; $n_0 t = 300 \text{ cm}^{-3} \text{ yr}$), the known age of the remnant, and the ambient density estimates of Toor (1980; $n_0 = 0.3 \text{ cm}^{-3}$) and Vink et al. (2000; $n_0 \sim 0.1 \text{ cm}^{-3}$). Willingale et al. (1996) find a somewhat larger ambient density [$n_0 = 0.52 \pm 0.08(d/1.7 \text{ kpc})^{1/2} \text{ cm}^{-3}$], and Dwarkadas & Chevalier (1998) report a somewhat lower density ($n_0 = 0.05\text{--}0.1 \text{ cm}^{-3}$). Although the remnant is interacting with a relatively dense environment in the northwest ($n_0 \approx 1 \text{ cm}^{-3}$; Winkler & Long 1997), the average ambient density at a Galactic height of 430 pc is about 0.06 cm^{-3} (Boulares & Cox 1990). Therefore, the average ambient density around SN 1006 may be about 0.1 cm^{-3} .

The inferred amount of shocked material $M_s = 8\text{--}67 M_\odot$. However, this range of values is an overestimate because the relative abundance of helium used in the best-fit model (Table 2) is the same as the relative abundance of helium in the solar system. Since Savedoff & Van Horn (1982) and Burleigh et al. (2000) report much smaller densities of helium in the neighborhood of SN 1006, a more appropriate abundance may be about 0.2 times the solar abundance. In this case, the best-fit amount of shocked material $M_s = 6.8 M_\odot$, and the 90% confidence level range is $6\text{--}47 M_\odot$. This range is consistent with the mass estimates of Pye et al. (1981; $M_s = 5\text{--}15 M_\odot$) and Vink et al. (2000; $M_s = 8.3 \pm 0.8 M_\odot$). However, the results of Dwarkadas & Chevalier (1998) suggest a somewhat smaller mass ($M_s = 3\text{--}5$) and Willingale et al. (1996) obtain a much smaller mass [$M_s = 1(d/1.7 \text{ kpc})^{1/2} M_\odot$]. With the exception of the estimate of Willingale et al. (1996), the mass estimates are substantially larger than the Chandrasekhar mass. Therefore, most of the hot shocked material is probably forward-shocked interstellar matter.

Unlike the parameters inferred from the thermal component of the BPL+NEI model, most of the parameters inferred from the thermal component of the BPL+RS model are inconsistent with the results of other observations. For example, the inferred velocity of the forward shock $v_{\text{fs}} = (16kT/3\mu)^{1/2} = 395\text{--}420 \text{ km s}^{-1}$ and the inferred ambient density $n_0 = 0.006\text{--}0.014 \text{ atoms cm}^{-3}$. These estimates are about an order of magnitude smaller than the results of previously published analyses. The values inferred for most of the other parameters listed in Table 3 are also unrealistic for the Raymond-Smith component of the BPL+RS model. Therefore, the Raymond-Smith model

provides a poor description of the thermal emission of SN 1006. The differences in the physical properties of the Raymond-Smith and nonequilibrium ionization models in XSPEC are that the Raymond-Smith model is based on the assumptions that the plasma is in a state of collisional ionization equilibrium and that the electron and ion temperatures have equilibrated. Neither of these two conditions is assumed for the nonequilibrium ionization model. In fact, at least one of the assumptions is not appropriate for SN 1006. Laming et al. (1996) show that the electron temperature is significantly smaller than the temperature of the ions in the northwest ($kT_e < 0.2kT_i$). This difference in the temperatures could explain why the parameters inferred from the Raymond-Smith model are inconsistent with other results.

Table 4 lists estimates of the kinetic energy of the matter in the remnant, E_{kin} , the thermal energy of the shock-heated protons, E_{kT_p} , and electrons, E_{kT_e} , the energy in the magnetic field, E_B , and the energy in cosmic rays, E_{cr} . Some of these estimates are based on the assumptions that the remnant is in a Sedov phase (Hamilton et al. 1983) and that the initial kinetic energy of the ejecta $E_0 = 10^{51}$ ergs. The scaling of the estimates with E_0 is indicated in the table. However, the results for SN 1006 may be insensitive to the assumption that the remnant is in a Sedov phase. For example, Dwarkadas & Chevalier (1998) suggest that SN 1006 has not yet reached the Sedov phase. The results of their analysis suggest that $M_s \approx 4 M_\odot$, $n_0 \approx 0.07 \text{ cm}^{-3}$, $r_{\text{fs}} = 8.5 \text{ pc}$, and $v_{\text{fs}} = 4000 \text{ km s}^{-1}$. If these values (instead of the values in Table 3) are used to compute the parameters in Table 4, $E_{\text{kin}} = 4 \times 10^{50}$ ergs and $E_{kT_p} = 4 \times 10^{50}$ ergs. Therefore, the same distribution of energy is obtained using the results of Dwarkadas & Chevalier (1998) because the smaller estimates of the amount of shocked material and the ambient density are offset by the larger estimates of the shock radius and velocity.

4.2. Nonthermal Emission

The high-energy X-ray emission from the northeastern and southwestern rims of SN 1006 is almost certainly nonthermal. An attempt to describe this emission using only thermal bremsstrahlung emission (Hamilton et al. 1983) was unsuccessful (Laming 1998). As described in section 2, the suggestion that the emission is associated with electrons beamed from an unseen central object is untenable. Reynolds (1996) argues convincingly that the only plausible explanation of the emission is synchrotron radiation from electrons accelerated to energies of about 10–100 TeV. This conclusion is supported by the results of the present analysis, which show that the nonthermal spectrum steepens with increasing energy (Fig. 6).

Figure 7 displays a compilation of the radio flux-density results of Kundu (1970), Milne (1971), Milne & Dickel (1975), Stephenson, Clark, & Crawford (1977), and Roger et al. (1988). The radio data can be fitted with a power law spectrum: $S_\nu = (17.9 \pm 1.1)(\nu/1 \text{ GHz})^{-0.57 \pm 0.06} \text{ Jy}$. The results of analyses of data obtained using the *IRAS* (Arendt 1989), *ROSAT* PSPC, *RXTE* PCA, *EGRET* (Hartman et al. 1999), *CANGAROO* (Tanimori et al. 1998), and *JANZOS* (Allen et al. 1995) instruments are also shown. The figure includes estimates of the photon spectra associated with

synchrotron radiation, inverse Compton scattering of the cosmic microwave background radiation, nonthermal bremsstrahlung, and the decay of neutral pions Gaisser, Protheroe, & Stanev (1998). The synchrotron spectrum is extrapolated from the radio data to X-ray energies assuming that the electron spectrum is as described in section 4.3. The nonthermal bremsstrahlung and π^0 spectra were computed assuming the density of protons in the remnant is 0.7 cm^{-3} . The nonthermal X-ray spectrum is consistent with a model of synchrotron radiation, but it is not consistent with models of nonthermal bremsstrahlung or inverse Compton scattering. The TeV gamma-ray data can be described by inverse Compton scattering.

As illustrated in Figure 7, the detection of X-ray synchrotron emission from SN 1006 requires the emission of synchrotron radiation at all energies between radio frequencies and X rays. Winkler & Long (1997) report the detection of faint diffuse emission ($\approx 1.0\text{--}2.5 \times 10^{-17} \text{ erg cm}^{-2} \text{ s}^{-1} \text{ arcsec}^{-2}$) in the $\text{H}\alpha$ band around the entire circumference of the remnant. Reynolds (1996) notes that the surface brightness of the synchrotron emission is about 28–32 mag arcsec $^{-2}$ in the visible band. This range corresponds to a flux of $0.1\text{--}6 \times 10^{-17} \text{ erg cm}^{-2} \text{ s}^{-1} \text{ arcsec}^{-2}$ in the $\text{H}\alpha$ band. Therefore, some of the faint diffuse $\text{H}\alpha$ flux may be produced by synchrotron radiation from electrons that have energies of about 1 TeV. The measurement of the optical (or infrared) synchrotron flux would be very important because it would corroborate the claim that the high-energy X-ray emission is synchrotron emission and could help determine the shape of the cosmic-ray electron spectrum of SN 1006.

As shown in Figure 7, the synchrotron and inverse Compton spectra of SN 1006 have similar shapes. Gamma-ray emission is detected near the peak of the inverse Compton spectrum. The electrons that produce this emission are the same electrons that produce the emission near the peak of the synchrotron spectrum. Therefore, the gamma-ray and nonthermal X-ray emission are produced by electrons that have similar energies. For this reason, the nonthermal X-ray and gamma-ray images are expected to be similar. Tanimori et al. (1998) report the detection of gamma rays from only the northeastern rim of SN 1006. The 95% confidence level upper limit on the gamma-ray flux from the southwestern rim ($1.1 \times 10^{-12} \text{ cm}^{-2} \text{ s}^{-1}$ at energies above 1.7 TeV) is no larger than about 40% of the flux of the northeastern rim [$(4.6 \pm 0.6 \pm 1.4) \times 10^{-12} \text{ cm}^{-2} \text{ s}^{-1}$ at energies above 1.7 TeV]. However, the nonthermal X-ray fluxes of the northeastern and southwestern rims are comparable. This discrepancy can be explained if the electron spectra, magnetic field strengths, or synchrotron and inverse Compton emission-angle distributions of the two rims are different. Of these possibilities, the X-ray data can be used to search for differences in the shapes of the electron spectra by searching for differences in the shapes of the synchrotron spectra of the two rims. Figure 8 shows a comparison of the nonthermal X-ray spectra of the two rims. For the purposes of this comparison, only the *ROSAT* PSPC data were used. The PSPC spectra of each rim were fitted with a model that includes a power law component ($dN/dE = F(E/1 \text{ keV})^{-\Gamma}$) and the thermal component described in Table 2. The ratio of the nonthermal X-ray fluxes of the southwestern and northeastern rims $f(E) = (F_{\text{SW}}/F_{\text{NE}})(E/1 \text{ keV})^{\Gamma_{\text{NE}}-\Gamma_{\text{SW}}}$. The 1, 2, and 3 σ confidence level contours for the parameter space defined by $F_{\text{SW}}/F_{\text{NE}}$ and $\Gamma_{\text{NE}} - \Gamma_{\text{SW}}$ are shown

in Figure 8. Since the point defined by $F_{\text{SW}}/F_{\text{NE}} = 1$ and $\Gamma_{\text{NE}} - \Gamma_{\text{SW}} = 0$ is well inside the 1σ confidence contour, there is no reason to believe that the shapes of the nonthermal X-ray spectra of the two rims are different in the energy range to which the *ROSAT* PSPC is sensitive. The results of the present analysis of the *RXTE* PCA data of the two rims also suggest that the shapes of the nonthermal X-ray spectra of the two rims are consistent with each other in the energy range to which the PCA is sensitive. Figure 8 includes curves along which the ratio f is a constant. Here, an energy $E = 0.1$ keV is used to compute the value of f , because we expect that the synchrotron emission at 0.1 keV and the TeV emission are produced by electrons that have the same energies. At the 3σ confidence level, the nonthermal flux from the southwestern rim at 0.1 keV is greater than 50% of the nonthermal flux from the northeastern rim at this energy. At face value, this lower limit seems to be inconsistent with the upper limit of 40% on the ratio of the gamma-ray fluxes. However, a significant difference between the electron spectra of the two rims produces a significant difference in the corresponding inverse Compton spectra, but only a modest difference in the synchrotron spectra. Therefore, the modest constraint on the ratio of the inverse Compton fluxes corresponds to a poor constraint on the ratio of the synchrotron fluxes of the two rims, and the results of the present analysis cannot exclude the possibility that the differences between the X-ray and gamma-ray images are due to differences between the electron spectra of the two rims. Perhaps this issue will be settled after the TeV and X-ray spectra of the two rims are better measured.

4.3. Cosmic Rays

The available radio and X-ray data for SN 1006 can be used to infer the parameters of the spectrum of the cosmic-ray electrons producing the synchrotron emission. For simplicity, the relativistic electron spectrum is assumed to have the form $dn_e/dE = A_e E^{-\Gamma_e} \exp(-E/\epsilon_e)$. This form is the high-energy limit of Bell’s (1978) expression:

$$dn/dE = Ag(E, m, \Gamma, \epsilon) \quad (1)$$

$$= A(E + mc^2)(E^2 + 2mc^2 E)^{-(\Gamma+1)/2} \exp(-E/\epsilon), \quad (2)$$

where $E [= (\gamma - 1)mc^2]$ is the kinetic energy of the particles and the exponential cutoff is added to the formula of Bell. The electron spectral index Γ_e can be determined from the spectral index of the radio data: $\Gamma_e = 2\alpha + 1 = 2.14 \pm 0.12$. However, estimates of the normalization factor A_e and the exponential cutoff energy ϵ_e of the electrons cannot be uniquely determined from the synchrotron data alone because the normalization ($S_\nu \propto A_e B^{1+\alpha}$) and the roll-off energy ($E_{\text{roll}} \propto \epsilon_e^2 B$) of the synchrotron spectrum depend on the strength of the magnetic field. (Note that $E_{\text{roll}} = 0.1$ keV in Fig. 7.) Since the normalization of the inverse Compton spectrum produced by the relativistic electrons depends on A_e (and the known spectrum of the cosmic microwave background radiation), but not B , the TeV gamma-ray data can be used to determine A_e . Then the flux and the roll-off energy of the synchrotron spectrum can be used to determine B and ϵ_e , respectively. For

example, if the cosmic-ray electrons and the magnetic field of SN 1006 have effective volume-filling factors $f_e = f_B = 0.25$, if the volume of the remnant $V = \frac{4}{3}\pi\theta^3 d^3 = 5 \times 10^{58} \text{ cm}^3$, and if the inverse Compton emission is dominated by scattering of the cosmic microwave background radiation, $A_e = 8.6 \times 10^{-9} \text{ cm}^{-3} \text{ GeV}^{\Gamma-1}$, $B = 10 \text{ } \mu\text{G}$, and $\epsilon_e = 20 \text{ TeV}$. Similar estimates of the magnetic field strength are reported by Tanimori et al. (1998; $B = 6.5 \pm 2 \text{ } \mu\text{G}$), Aharonian & Atoyan (1999; $B = 10 \text{ } \mu\text{G}$), and Dyer et al. (2001a, $B = 10 \text{ } \mu\text{G}$). However, these estimates of the magnetic field strength seem rather small. If the field strength at a Galactic height of 430 pc is similar to the strength in the plane (Boulares & Cox 1990), a field of $10 \text{ } \mu\text{G}$ can be little more than a compressed ambient field. Yet, the large and abrupt change in the radio surface brightness in the regions of the bright rims of SN 1006 (Reynolds & Gilmore 1986), the presence of a radially oriented component of the field (Reynolds & Gilmore 1993), and estimates of the total energy in cosmic-ray particles (described below) suggest that the field has been significantly amplified. Perhaps one or more of the assumptions used to determine the strength of the magnetic field is wrong. In particular, the effective volume-filling factor of the magnetic field may be smaller than the filling factor of the cosmic rays (Jun & Jones 1999). In this case, the magnetic field strength is underestimated. For example, if $f_e = 0.25$ and $f_B = 0.1$, $A_e = 2.4 \times 10^{-9} \text{ cm}^{-3} \text{ GeV}^{\Gamma-1}$, $B = 40 \text{ } \mu\text{G}$, and $\epsilon_e = 10 \text{ TeV}$. This value for the magnetic field lies comfortably between the compressed value ($B \approx 10 \text{ } \mu\text{G}$) and the value obtained using the minimum-energy condition ($B \approx 100 \text{ } \mu\text{G}$). For the remainder of the discussion, it is assumed that $B = 40 \text{ } \mu\text{G}$ and that the cosmic-ray electron spectrum is specified by equation (2), where A_e , Γ_e , and ϵ_e are listed in Table 5. The inferred spectrum of cosmic-ray electrons is shown in Figure 9.

Although there is no evidence that cosmic-ray nuclei are accelerated in SN 1006 (cf. Aharonian & Atoyan 1999), Ellison & Reynolds (1991) suggest that relativistic electrons and nuclei are accelerated in a similar manner. Therefore, we estimate the parameters of the cosmic-ray nuclei spectra. For simplicity, only hydrogen and helium nuclei are considered. The nonthermal spectra of these particles are assumed to have the same functional form as equation (2). The spectral indices of the protons and alpha particles are assumed to be the same as the spectral index of the electrons ($\Gamma_p = \Gamma_{\text{He}} = \Gamma_e = 2.14$). The exponential cutoff energies of the different cosmic-ray particles are assumed to be related by the magnetic rigidity of the particles (i.e., $\epsilon_p = \frac{1}{2}\epsilon_{\text{He}} = \epsilon_e = 10 \text{ TeV}$). This relationship is appropriate if the maximum energy of the electrons is limited by the escape of the particles from the remnant (Reynolds 1996; Dyer et al. 2001a), but it is not appropriate if ϵ_e is limited by radiative losses. The values of A_p and A_{He} are determined using the value of A_e and the technique described below. The ratio of the number density of protons to helium nuclei $n_p : n_{\text{He}} = 1 : 0.02$ in the neighborhood of SN 1006 (Savedoff & Van Horn 1982; Burleigh et al. 2000). If the shocked protons and helium atoms are fully ionized, then $n_e = 1.04n_p$. (The electron contribution from other nuclei is expected to be small.) Therefore, $n_p : n_{\text{He}} : n_e = 1 : 0.02 : 1.04$. The fractional numbers of nonthermal protons and helium nuclei are assumed to be the same as the fractional number of nonthermal electrons (i.e., $\eta \equiv n_p^{\text{cr}}/n_p = n_{\text{He}}^{\text{cr}}/n_{\text{He}} = n_e^{\text{cr}}/n_e$). Using this

relationship and the equations

$$n_p^{\text{cr}} = A_p \int_{E_{\min,p}}^{E_{\max,p}} dE g(E, m_p, \Gamma_p, \epsilon_p) \quad (3)$$

and

$$n_e^{\text{cr}} = A_e \int_{E_{\min,e}}^{E_{\max,e}} dE g(E, m_e, \Gamma_e, \epsilon_e) \quad (4)$$

yields

$$A_p = A_e \frac{n_p \int_{E_{\min,e}}^{E_{\max,e}} dE g(E, m_e, \Gamma_e, \epsilon_e)}{n_e \int_{E_{\min,p}}^{E_{\max,p}} dE g(E, m_p, \Gamma_p, \epsilon_p)} \quad (5)$$

$$= 1.1 \times 10^{-6} \text{ cm}^{-3} \text{ GeV}^{\Gamma-1}, \quad (6)$$

where $E_{\min,e} = 0.58 \text{ keV}$, $E_{\max,e} = \epsilon_e = 10 \text{ TeV}$, $E_{\min,p} = \frac{3}{16} m_p v_{\text{fs}}^2 = 14 \text{ keV}$, and $E_{\max,p} = \epsilon_p = 10 \text{ TeV}$. Similarly,

$$A_{\text{He}} = A_e \frac{n_{\text{He}} \int_{E_{\min,e}}^{E_{\max,e}} dE g(E, m_e, \Gamma_e, \epsilon_e)}{n_e \int_{E_{\min,He}}^{E_{\max,He}} dE g(E, m_{\text{He}}, \Gamma_{\text{He}}, \epsilon_{\text{He}})} \quad (7)$$

$$= 1.0 \times 10^{-7} \text{ cm}^{-3} \text{ GeV}^{\Gamma-1}, \quad (8)$$

where $E_{\min,He} = \frac{3}{16} m_{\text{He}} v_{\text{fs}}^2 = 57 \text{ keV}$ and $E_{\max,He} = \epsilon_{\text{He}} = 20 \text{ TeV}$. The parameters of the cosmic-ray proton and helium spectra are listed in Table 5, and the spectra are shown in Figure 9. These parameters and equation (2) yield a cosmic-ray injection efficiency $\eta = 5 \times 10^{-4}$ if the magnetic field $B = 40 \mu\text{G}$. This efficiency is assumed to be the same for all particle species. Our assumptions about the shapes of the cosmic-ray spectra and about the relative numbers of nonthermal protons and electrons yield a number density of protons that is 160 times larger than the number density of electrons at 1 GeV (i.e., $dn_p^{\text{cr}}/dE = 160 dn_e^{\text{cr}}/dE$ at 1 GeV; Fig. 9). Within the rather large uncertainties of our estimates, this ratio is consistent with the ratio observed at Earth (Meyer 1969).

The energies in cosmic-ray electrons, protons, and helium nuclei can be obtained from equation (2) and the particle-spectra parameters listed in Table 5 and above:

$$\begin{aligned} E_e &= V \int_{E_{\min,e}}^{E_{\max,e}} dE E A_e g(E, m_e, \Gamma_e, \epsilon_e) \\ &= 9 \times 10^{47} \text{ ergs}, \end{aligned} \quad (9)$$

$$\begin{aligned} E_p &= V \int_{E_{\min,p}}^{E_{\max,p}} dE E A_p g(E, m_p, \Gamma_p, \epsilon_p) \\ &= 1 \times 10^{50} \text{ ergs, and} \end{aligned} \quad (10)$$

$$\begin{aligned} E_{\text{He}} &= V \int_{E_{\min,He}}^{E_{\max,He}} dE E A_{\text{He}} g(E, m_{\text{He}}, \Gamma_{\text{He}}, \epsilon_{\text{He}}) \\ &= 8 \times 10^{48} \text{ ergs.} \end{aligned} \quad (11)$$

The sum of these three energies is $E_{\text{cr}} = 1 \times 10^{50}$ ergs. As expected, the cosmic-ray energy is dominated by the energy in cosmic-ray protons. The estimates of the cosmic-ray and magnetic field energies are listed in Table 4 for the case in which $B = 40 \mu\text{G}$. Dyer et al. (2001a) estimate the energy in only cosmic-ray electrons and obtain an energy that is about an order of magnitude larger than 9×10^{47} ergs because they used a magnetic field of about $10 \mu\text{G}$ instead of the field strength of $40 \mu\text{G}$ used here.

Drury et al. (1989) and Markiewicz et al. (1990) modeled the evolution of a supernova remnant using conditions that are quite similar to the conditions appropriate for SN 1006. These authors assume that $1 M_{\odot}$ of material is ejected with an initial kinetic energy of $E_0 = 1\text{--}2 \times 10^{51}$ ergs into an ambient medium that has a density $n_0 = 0.1 \text{ cm}^{-3}$. The predicted results for the case in which the injection efficiency $\epsilon = 10^{-3}$ (Fig. 3 of Drury et al. 1989 and Fig. 4 of Markiewicz et al. 1990) are consistent with our estimates of the distribution of energy between thermal particles, cosmic rays, and kinetic energy (Table 4). Note that the cosmic-ray injection efficiency parameter ϵ of Drury et al. (1989) and Markiewicz et al. (1990), which should not be confused with our use of ϵ for the exponential cutoff energy of the cosmic-ray spectra, is computed somewhat differently from the injection efficiency parameter η used here. If $B = 40 \mu\text{G}$, $\eta = 5 \times 10^{-4}$ and the corresponding value of $\epsilon = 1 \times 10^{-3}$. Therefore, our results and those of Drury et al. (1989) and Markiewicz et al. (1990) are consistent if the magnetic field is about $40 \mu\text{G}$. If the magnetic field strength is as small as $10 \mu\text{G}$, $\eta = 2 \times 10^{-3}$, $\epsilon = 4 \times 10^{-3}$, and the total energy in cosmic rays $E_{\text{cr}} = 4 \times 10^{50}$ ergs (i.e., the energy is expected to be more or less equally distributed between kinetic energy, thermal energy, and cosmic rays). For comparison, Figures 2 and 3 of Drury et al. (1989) suggest that almost all of the energy would be contained in the cosmic rays if $\epsilon = 4 \times 10^{-3}$. Therefore, the results of Drury et al. (1989) are more compatible with a magnetic field of $40 \mu\text{G}$ than a field of $10 \mu\text{G}$.

The estimates of the parameters of the cosmic-ray spectra of SN 1006 have important implications for Galactic cosmic-ray acceleration. It is generally accepted that Galactic cosmic rays are accelerated predominantly in the shocks of supernova remnants. If this hypothesis is true, an average supernova remnant should transfer a sufficient amount of energy to cosmic rays, produce a cosmic-ray proton spectrum that has an appropriate spectral index, and accelerate protons to energies high enough to explain the properties of the cosmic rays observed at Earth. Since the average flux of cosmic rays in the solar system has been constant within a factor of 2 over the last 10^9 yr (Reedy, Arnold, & Lal 1983), the mean rate at which cosmic rays are energized should be approximately equal to the rate at which energy is lost as cosmic rays diffuse from the Galaxy. This rate ($\dot{E}_{\text{loss}} = 0.3\text{--}1 \times 10^{41} \text{ ergs s}^{-1}$; Parker 1969; Blandford & Eichler 1987; Drury et al. 1989; Lingelfelter 1992) and the assumption that one supernova remnant occurs every 30 yr suggest that an average supernova remnant produces $0.3\text{--}1 \times 10^{50}$ ergs of cosmic rays over the lifetime of the remnant (i.e., 3%–10% of the initial kinetic energy of the ejecta is transferred to cosmic rays). The estimate of the cosmic-ray energy in SN 1006 at the present is already consistent with this range if $B \leq 100 \mu\text{G}$. Therefore, the total energy of the cosmic-ray protons in SN 1006 may be consistent

with the energy inferred for the sources of Galactic cosmic rays.

The average spectral index of the relativistic cosmic-ray proton spectra produced by the accelerators of Galactic cosmic rays ($\Gamma_p = 2.2$) is inferred from the spectral index of the cosmic-ray proton spectrum observed at Earth ($\Gamma_p = 2.80 \pm 0.04$; Asakimori et al. 1998) and the spectral steepening due to the energy-dependent escape of cosmic rays from the Galaxy ($\Delta\Gamma = 0.6$; Swordy et al. 1990). The radio synchrotron flux of SN 1006 is produced by electrons that have energies of about 1 GeV. At these energies the spectral index of the cosmic-ray electrons $\Gamma_e = 2.14 \pm 0.12$. Since relativistic protons and electrons are thought to be accelerated in a similar manner, the relativistic proton spectrum of SN 1006 may have a spectral index that is consistent with the index inferred for the accelerators of Galactic cosmic rays.

The spectral index of the all-particle cosmic-ray spectrum observed at Earth is more or less the same up to an energy of about 3000 TeV. Above this energy, the spectrum gradually steepens to have an index of about 3. Since the observed cosmic rays that have energies below this “knee” feature are thought to be Galactic, the Galactic cosmic-ray accelerators are expected to be capable of accelerating particles to energies as high as 3000 TeV. If the mechanism responsible for the acceleration of Galactic cosmic rays depends on the magnetic rigidity of the particles (which is true for diffusive shock acceleration in supernova remnants), it may be the case that the cosmic-ray particles at 3000 TeV are principally iron and that protons are accelerated to energies of only about 100 TeV (Lagage & Cesarsky 1983). The estimated cutoff energy of the electron spectrum of SN 1006 ($\epsilon_e = 10$ TeV), while uncertain, is lower than 100 TeV. Since relativistic electrons and protons that have the same energy have the same magnetic rigidity, the maximum energy of the protons is expected to be the same as the maximum energy of the electrons unless the maximum energy of the electrons is regulated by radiative losses. If the magnetic field $B = 40 \mu\text{G}$, an electron with an energy $E = \epsilon_e = 10$ TeV radiates half of its energy in about 400 yr. Since this time is less than the age of the remnant, the maximum energy of shock-accelerated electrons may be limited by synchrotron losses. In this case, the value of the energy ϵ_e represents a lower limit on the exponential cutoff energy of the proton spectrum because radiative losses are only important for electrons, not nuclei. Therefore, the maximum energy of the protons may be consistent with the expected value of $\epsilon_p = 100$ TeV. However, if the magnetic field strength $B = 10 \mu\text{G}$, the time required for a 20 TeV electron to radiate half of its energy (3000 yr) is significantly greater than the age of the remnant. If the magnetic field is this small, the maximum energy of the electrons in SN 1006 may be regulated by the free escape of the particles from the remnant (Reynolds 1996; Dyer et al. 2001a). In this case, the maximum energy of the protons is the same as the maximum energy of the electrons and is well below the expected energy of 100 TeV.

5. Conclusion

We present the results of a spectral analysis of *RXTE* PCA, *ASCA* SIS, and *ROSAT* PSPC data of the supernova remnant SN 1006. These data were fitted with several sets of thermal and

nonthermal X-ray emission models to characterize the global spectral properties of the remnant. The present work represents the first attempt to model both the thermal and nonthermal X-ray emission over the entire X-ray energy band from 0.12–17 keV.

The best-fit model includes a nonequilibrium ionization component and a broken power law component, which are absorbed through an interstellar column density $n_{\text{H}} = 5.6 \times 10^{20} \text{ atoms cm}^{-2}$. The thermal component is described by an electron temperature $kT_e = 0.6 \text{ keV}$ and an ionization timescale $n_0 t = 9 \times 10^9 \text{ cm}^{-3} \text{ s}$. The large relative elemental abundance of silicon (10–18 times larger than the relative elemental abundance of silicon in the solar system) indicates that most of the X-ray-emitting silicon is reverse-shocked ejecta. The inferred mass of the shocked material is several times larger than the Chandrasekhar mass, which implies that most of the shocked material is interstellar.

The nonthermal X-ray emission is well described by a broken power law component with a low-energy photon index $\Gamma_1 = 2.1$ and a high-energy photon index $\Gamma_2 = 3.0$. Since Γ_2 is significantly larger than Γ_1 , the broken power law represents an approximation to a nonthermal spectrum that is steepening with increasing energy. This result supports previous claims that the nonthermal X-ray emission from SN 1006 is produced by synchrotron radiation from very high energy electrons. Using both the radio and X-ray synchrotron results, the spectrum of relativistic electrons in the remnant is inferred to have the form $dn_e/dE = A_e E^{-\Gamma_e} \exp(-E/\epsilon_e)$, with $A_e = 2.4 \times 10^{-9} \text{ cm}^{-3} \text{ GeV}^{\Gamma-1}$, $\Gamma_e = 2.14 \pm 0.12$, and $\epsilon_e = 10 \text{ TeV}$. The values of A_e and ϵ_e are based on the assumption that the mean strength of the magnetic field in the synchrotron-emitting region $B = 40 \mu\text{G}$. This value was arbitrarily chosen for the present work because it is between the value obtained if the magnetic field is merely a compressed ambient field ($10 \mu\text{G}$) and the value obtained using the minimum-energy condition ($100 \mu\text{G}$). Other published estimates of the field strengths are near $10 \mu\text{G}$, but this value seems to be incompatible with the large, abrupt change in the radio flux at the bright rims, the detection of a significant radial component of the field, and the models of Drury et al. (1989).

Since SN 1006 is expected to accelerate cosmic-ray nuclei as well as electrons, we have also estimated the parameters of the proton and helium spectra. The results suggest that the number density of protons is 160 times larger than the number density of electrons at 1 GeV. This ratio is comparable to the ratio observed at Earth. Integrating over the nonthermal particle spectra yields an estimate of the total energy in cosmic rays $E_{\text{cr}} = 10^{50} \text{ ergs}$. This energy and the differential spectral index of the electrons at 1 GeV ($\Gamma_e = 2.14 \pm 0.12$) are consistent with the hypothesis that Galactic cosmic rays are accelerated predominantly in the shocks of supernova remnants. However, the maximum energy of cosmic-ray electrons in SN 1006 is well below 100 TeV ($\epsilon_e = 10 \text{ TeV}$). If the maximum energy of cosmic-ray protons $\epsilon_p = \epsilon_e$, the remnant does not accelerate particles to the energy of the “knee” at about 3000 TeV. Yet, if $B = 40 \mu\text{G}$, the maximum energy of the electrons may be limited by synchrotron losses and the maximum energy of nuclei might be significantly larger than 10 TeV. Therefore, SN 1006 is clearly a significant source of Galactic cosmic rays (at least cosmic-ray electrons), but the remnant may or may not be capable of accelerating particles to energies as high as the energy of the knee. Similar conclusions are reported for other young

Galactic shell-type remnants (Allen et al. 1997, 1999; Reynolds & Keohane 1999).

Unlike the X-ray and radio synchrotron emission, TeV gamma-ray emission is only observed from the northeastern rim of the remnant. One possible explanation for this discrepancy is that the two rims have different electron spectra. The results of the present analysis are consistent with the idea that the electron spectra of the two rims are the same, but the possibility that the spectra are different cannot be excluded. Therefore, the nature of this puzzle remains a mystery.

We thank Stephen Reynolds for many thoughtful and informative discussions about particle acceleration in supernova remnants and the photon emission processes of the accelerated particles. We are grateful for Matthew Baring’s suggestions about the distribution of energy in a supernova remnant. We thank John Houck for helpful discussions about the thermal emission properties of shocked plasmas and for carefully reviewing the manuscript. We appreciate the many useful suggestions of the anonymous referee that have helped improve the paper. The present work involved the use of the data analysis tools and data archives maintained by the HEASARC at NASA/Goddard Space Flight Center. This work was performed, in part, while G. E. A. held an NRC-NASA/GSFC Postdoctoral Research Associateship, and G. E. A. warmly acknowledges Keith Jahoda and the *RXTE* PCA team for their support and hospitality during his tenure at NASA/GSGC. The research efforts of G. E. A. are supported in part by the *Chandra* X-Ray Center under contract SVI-61010 with the Smithsonian Astrophysical Observatory.

REFERENCES

- Aharonian, F. A., & Atoyan, A. M. 1999, *A&A*, 351, 330
- Allen, G. E., Gotthelf, E. V., & Petre, R. 1999, in *Proc. 26th Int. Cosmic Ray Conf. (Salt Lake City)*, 3, 480 (available at <http://xxx.lanl.gov/abs/astro-ph/9908209>)
- Allen, G. E., et al. 1997, *ApJ*, 487, L97
- Allen, W. H., et al. 1995, in *Proc. 24th Int. Cosmic Ray Conf. (Rome)*, 2, 447
- Anders, E., & Grevesse, N. 1989, *Geochim. et Cosmochim. Acta*, 53, 197
- Arendt, R. G. 1989, *ApJS*, 70, 181
- Asakimori, K., et al. 1998, *ApJ*, 502, 278
- Becker, R. H., Szymkowiak, A. E., Boldt, E. A., Holt, S. S., & Serlemitsos, P. J. 1980, *ApJ*, 240, L33
- Bell, A. R. 1978, *MNRAS*, 182, 443
- Blandford, R. & Eichler, D. 1987, *Phys. Rep.*, 154, 1

- Bock, D. C.-J., Turtle, A. J., & Green, A. J. 1998, *AJ*, 116, 1886
- Borkowski, K. J., Rho, J., Reynolds, S. P., & Dyer, K. K. 2000, *ApJ*, submitted
- Boulares, A., & Cox, D. P. 1990, *ApJ*, 365, 544
- Burke, B. E., Mountain, R. W., Daniels, P. J., Cooper, M. J., & Dolat, V. S. 1994, *IEEE Trans. Nucl. Sci.*, 41, 375
- Burleigh, M. R., Heber, U., O’Donoghue, D., & Barstow, M. A. 2000, *A&A*, 356, 585
- Chevalier, R. A., & Raymond, J. C. 1978, *ApJ*, 225, L27
- Drury, L. O’C., Markiewicz, W. J., & Völk, H. J. 1989, *A&A*, 225, 179
- Dwarkadas, V. V., & Chevalier, R. A. 1998, *ApJ*, 497, 807
- Dyer, K. K., Reynolds, S. P., Borkowski, K. J., Allen, G. E., & Petre, R. 2001a, *ApJ*, 551, 439
- Dyer, K. K., Reynolds, S. P., Borkowski, K. J., & Petre, R. 2001b, in *AIP Conf. Ser.* 565, Young Supernova Remnants, ed. S. S. Holt & U. Hwang (New York: Springer)
- Ellison, D. C., & Reynolds, S. P. 1991, *ApJ*, 382, 242
- Fesen, R. A., Wu, C.-C., Leventhal, M., & Hamilton, A. J. S. 1988, *ApJ*, 327, 164
- Gaisser, T. K., Protheroe, R. J., & Stanev, T. 1998, *ApJ*, 492, 219
- Galas, C. M. F., Venkatesan, D., & Garmire, G. 1982, *Astrophys. Lett.*, 22, 103
- Hamilton, A. J. S., Fesen, R. A., Wu, C.-C., Crenshaw, D. M., & Sarazin, C. L. 1997, *ApJ*, 481, 838
- Hamilton, A. J. S., & Sarazin, C. L. 1984, *ApJ*, 287, 282
- Hamilton, A. J. S., Sarazin, C. L., & Chevalier, R. A. 1983, *ApJS*, 51, 115
- Hamilton, A. J. S., Sarazin, C. L., & Szymkowiak, A. E. 1986, *ApJ*, 300, 698
- Hartman, R. C. 1999, *ApJS*, 123, 79
- Hesser, J. E., & van den Bergh, S. 1981, *ApJ*, 251, 549
- Jahoda, K., Swank, J. H., Giles, A. B., Stark, M. J., Strohmayer, T., Zhang, W., & Morgan, E. H. 1996, *Proc. SPIE*, 2808, 59
- Jun, B.-I., & Jones, T. W. 1999, *ApJ*, 511, 774
- Kirshner, R. P., Winkler, P. F., & Chevalier, R. A. 1987, *ApJ*, 315, L135

- Koyama, K., Kinugasa, K., Matsuzaki, K., Nishiuchi, M., Sugizaki, M., Torii, K., Yamauchi, S., & Aschenbach, B. 1997, PASJ, 49, L7
- Koyama, K., Petre, R., Gotthelf, E. V., Hwang, U., Matsuura, M., Ozaki, M., & Holt, S. S. 1995, Nature, 378, 255
- Koyama, K., Tsunemi, H., Becker, R. H., & Hughes, J. P. 1987, PASJ, 39, 437
- Kundu, M. R. 1970, ApJ, 162, 17
- Lagage, P. O., & Cesarsky, C. J. 1983, A&A, 125, 249
- Laming, J. M. 1998, ApJ, 499, 309
- Laming, J. M., Raymond, J. C., McLaughlin, B. M., & Blair, W. P. 1996, ApJ, 472, 267
- Lampton, M., Margon, B., & Bowyer, S. 1976, ApJ, 208, 177
- Leahy, D. A., Nousek, J., & Hamilton, A. J. S. 1991, ApJ, 374, 218
- Lingenfelter, R. E. 1992, in The Astronomy & Astrophysics Encyclopedia, ed. S. Maran (New York: Van Nostrand & Reinhold Publishers), 65
- Long, K. S., Blair, W. P., & van den Bergh, S. 1988, ApJ, 333, 749
- Markiewicz, W. J., Drury, L. O’C., & Völk, H. J. 1990, A&A, 236, 487
- Markwardt, C. B., & Ögelman, H. 1995, Nature, 375, 40
- Mastichiadis, A., & de Jager, O. C. 1996, A&A, 311, L5
- Meyer, P. 1969, ARA&A, 7, 1
- Milne, D. K. 1971, Australian. J. Phys., 24, 757
- Milne, D. K., & Dickel, J. R. 1975, Australian. J. Phys., 28, 209
- Moffett, D. A., Goss, W. M., & Reynolds, S. P. 1993, AJ, 106, 1566
- Muraishi, H., et al. 2000, A&A, 354, L57
- Nomoto, K., Thielemann, F.-K., & Yokoi, K. 1984, ApJ, 286, 644
- Ozaki, M., Koyama, K., Ueno, S., & Yamauchi, S. 1994, PASJ, 46, 367
- Parker, E. N. 1969, Space Sci. Rev., 9, 651
- Pfeffermann, E., et al. 1987, Proc. SPIE, 733, 519
- Plucinsky, P. P., Snowden, S. L., Briel, U. G., Hasinger, G., & Pfeffermann, E. 1993, ApJ, 418, 519

- Pye, J. P., Pounds, K. A., Rolf, D. P., Seward, F. D., Smith, A., & Willingale, R. 1981, MNRAS, 194, 569
- Raymond, J. C., Blair, W. P., & Long, K. S. 1995, ApJ, 454, L31
- Raymond, J. C., & Smith, B. W. 1977, ApJS, 35, 419
- Reedy, R. C., Arnold, J. R., & Lal, D. 1983, Ann. Rev. Nucl. Part. Sci., 33, 505
- Reynolds, S. P. 1996, ApJ, 459, L13
- Reynolds, S. P., & Gilmore, D. M. 1986, AJ, 92, 1138
- . 1993, AJ, 106, 272
- Reynolds, S. P., & Keohane, J. W. 1999, ApJ, 525, 368
- Roger, R. S., Milne, D. K., Kesteven, M. J., Wellington, K. J., & Haynes, R. F. 1988, ApJ, 332, 940
- Savedoff, M. P., & Van Horn, H. M. 1982, A&A, 107, L3
- Schaefer, B. E. 1996, ApJ, 459, 438
- Slane, P., Gaensler, B. M., Dame, T. M., Hughes, J. P., Plucinsky, P. P., & Green, A. 1999, ApJ, 525, 357
- Slane, P., & Lloyd, N. 1995, ApJ, 452, L115
- Stephenson, F. R., Clark, D. H., & Crawford, D. F. 1977, MNRAS, 180, 567
- Swordy, S. P., Müller, D., Meyer, P., L’Heureux, J., & Grunsfeld, J. M. 1990, ApJ, 349, 625
- Tanaka, Y., Inoue, H., & Holt, S. S. 1994, PASJ, 46, L37
- Tanimori, T., et al. 1998, ApJ, 497, L25
- Toor, A. 1980, A&A, 85, 184
- Vartanian, M. H., Lum, K. S. K., & Ku, W. H.-M., 1985, ApJ, 288, L5
- Vink, J., Kaastra, J. S., Bleeker, J. A. M., & Preite-Martinez, A. 2000, A&A, 354, 931
- Vink, J., Maccarone, M. C., Kaastra, J. S., Mineo, T., Bleeker, J. A. M., Preite-Martinez, A., & Bloemen, H. 1999, A&A, 344, 289
- Willingale, R., West, R. G., Pye, J. P., & Stewart, G. C. 1996, MNRAS, 278, 749
- Winkler, P. F., Jr., Hearn, D. R., Richardson, J. A., & Behnken, J. M. 1979, ApJ, 229, L123

Winkler, P. F., Jr., & Laird, F. N. 1976, *ApJ*, 204, L111

Winkler, P. F., & Long, K. S. 1997, *ApJ*, 491, 829

Wu, C.-C., Crenshaw, D. M., Fesen, R. A., Hamilton, A. J. S., & Sarazin, C. L. 1993, *ApJ*, 416, 247

Yoshikoshi, T., et al. 1997, *ApJ*, 487, 65

Zarnecki, J. C., & Bibbo, G. 1979, *MNRAS*, 186, 51P

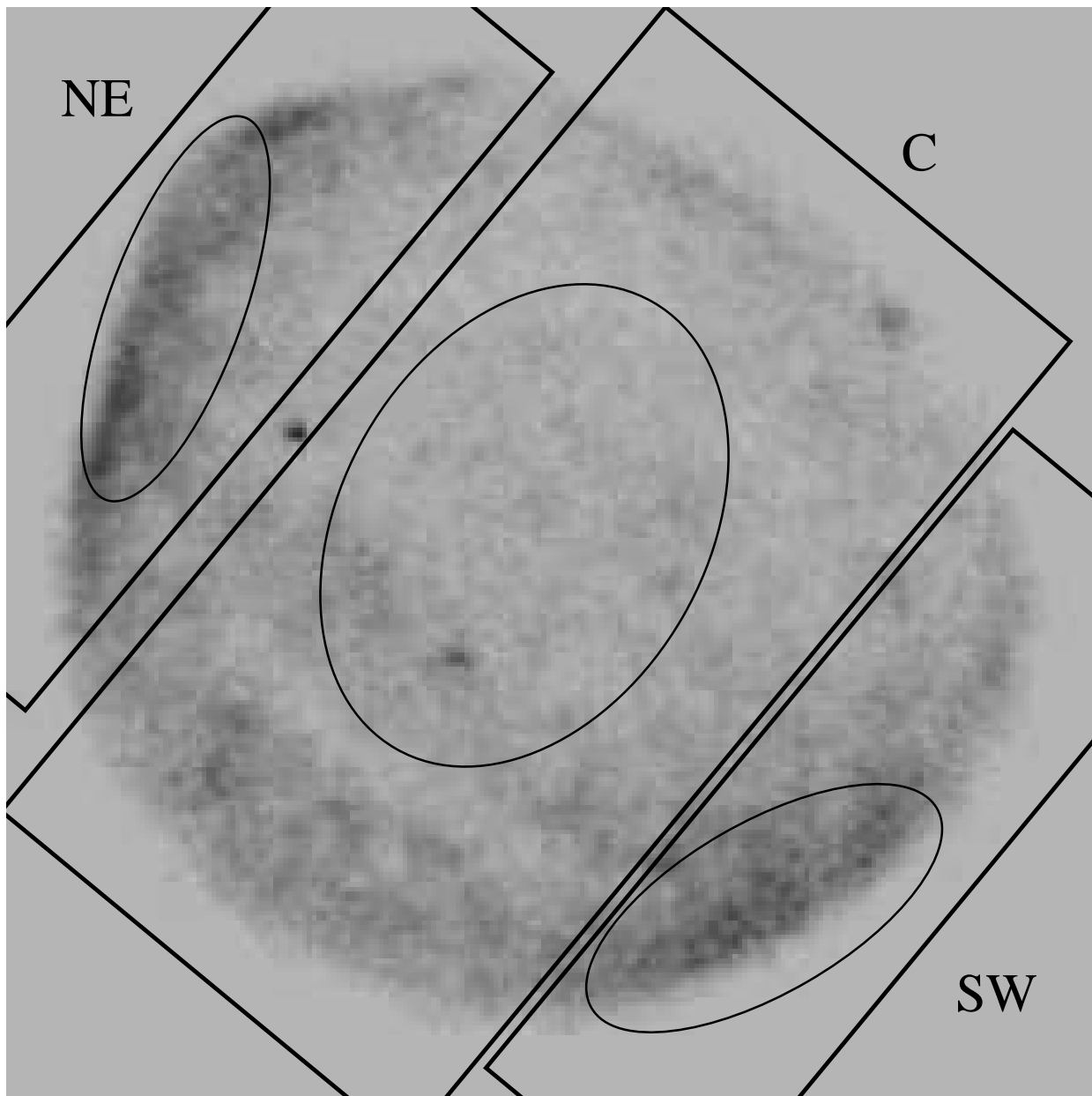


Fig. 1.— A *ROSAT* PSPC image of SN 1006. North is up and east is to the left. The three rectangles are the regions used to extract the PSPC spectra for the northeastern rim (NE), center of the remnant (C), and southwestern rim (SW). The three ovals are the regions used to extract the ASCA SIS spectra.

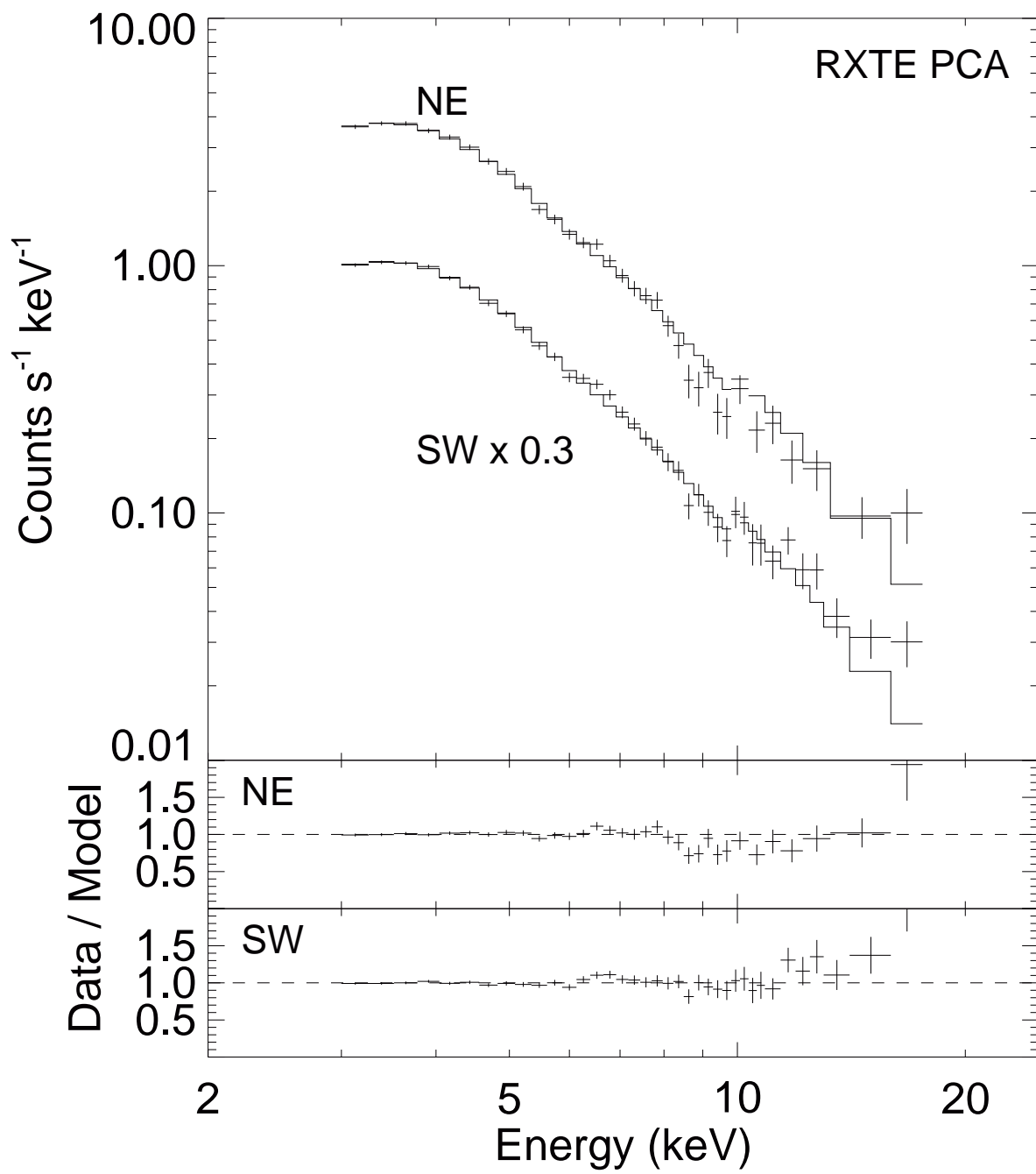


Fig. 2.— *RXTE* PCA data of SN 1006. The top panel includes data for pointings at the the northeastern (NE) and southwestern (SW) rims of the remnant. The entire remnant is in the field of view of the PCA at both pointing positions. The histograms through the data show the results of the best-fit model. The spectral data and model of the southwestern pointing have been multiplied by a factor of 0.3 for clarity. The bottom panels show the ratios of the data to the model for both pointings. The model describes the spectra quite well.

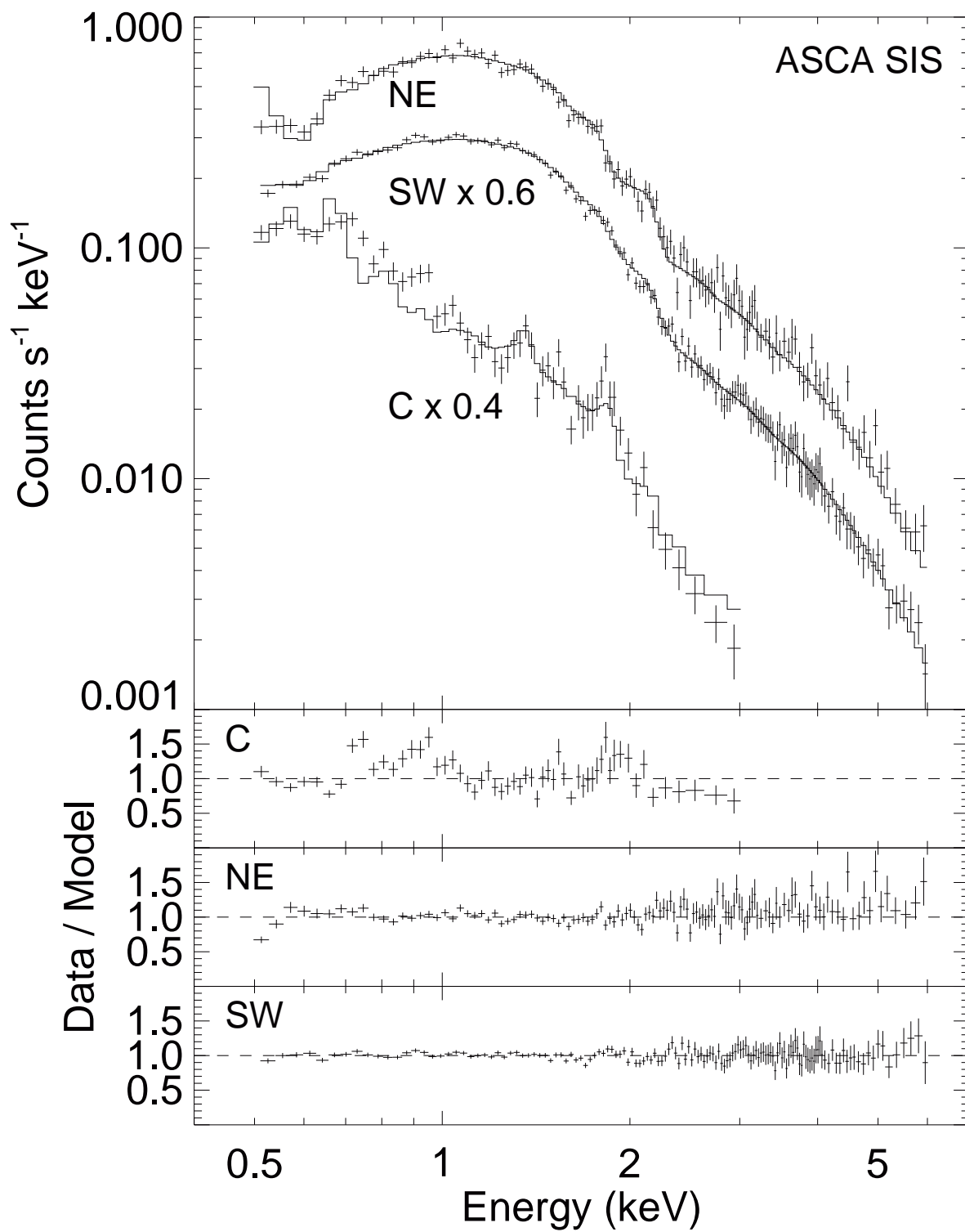


Fig. 3.— *ASCA* SIS data of SN 1006. The top panel includes data for spatially separate regions along the northeastern (NE) and southwestern (SW) rims and in the center of the remnant (C). The histograms through the data show the results of the best-fit model. The spectral data and models of the southwestern and central regions have been multiplied by factors of 0.6 and 0.4, respectively, for clarity. The bottom panels show the ratios of the data to the model. In general, the model describes the spectra quite well.

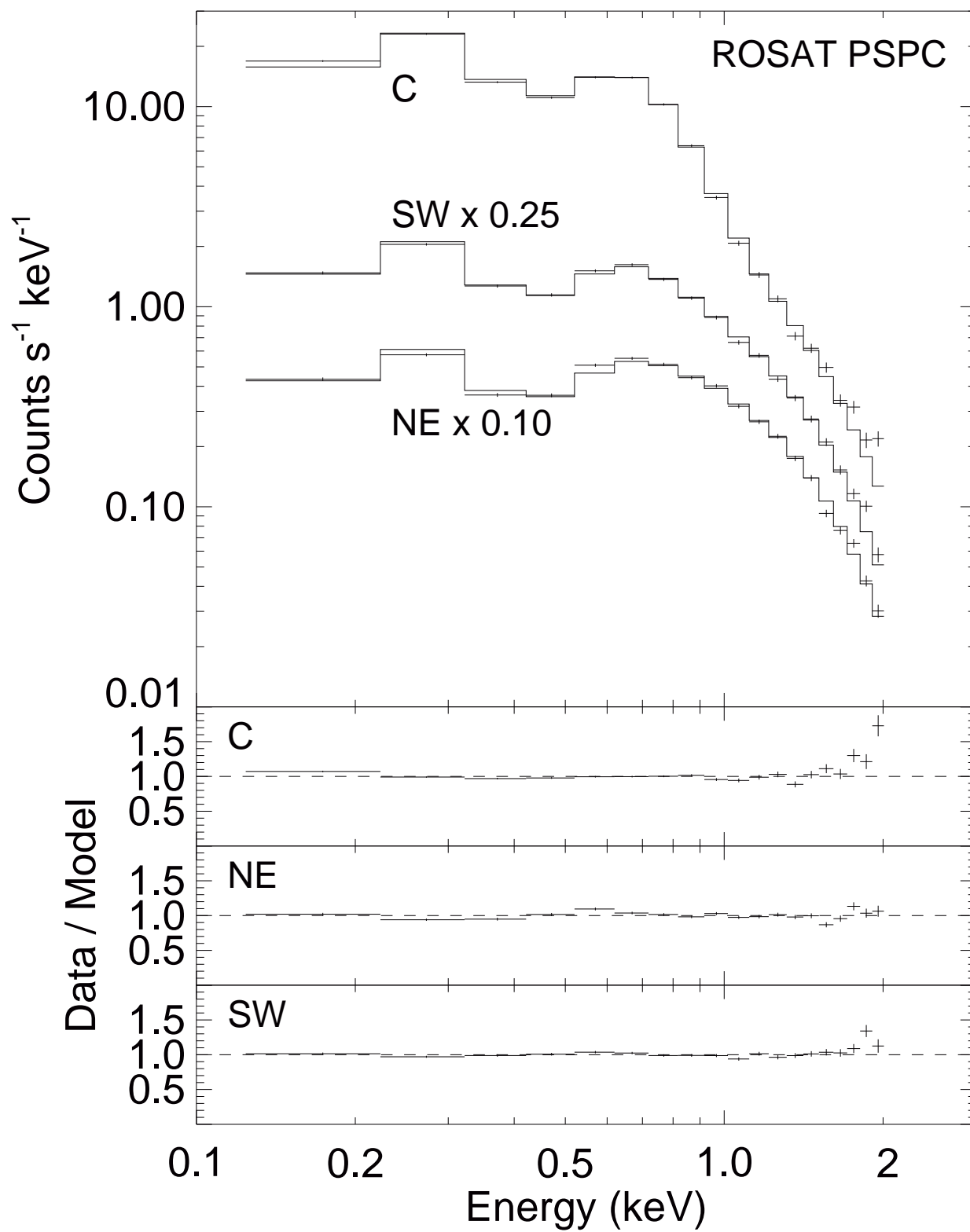


Fig. 4.— *ROSAT* PSPC data of SN 1006. The top panel includes data for spatially separate regions in the center of the remnant (C) and along the southwestern (SW) and northeastern (NE) rims. The histograms through the data show the results of the best-fit model. The spectral data and models of the southwestern and northeastern regions have been multiplied by factors of 0.25 and 0.10, respectively, for clarity. The bottom panels show the ratios of the data to the model. The model describes the spectra quite well.

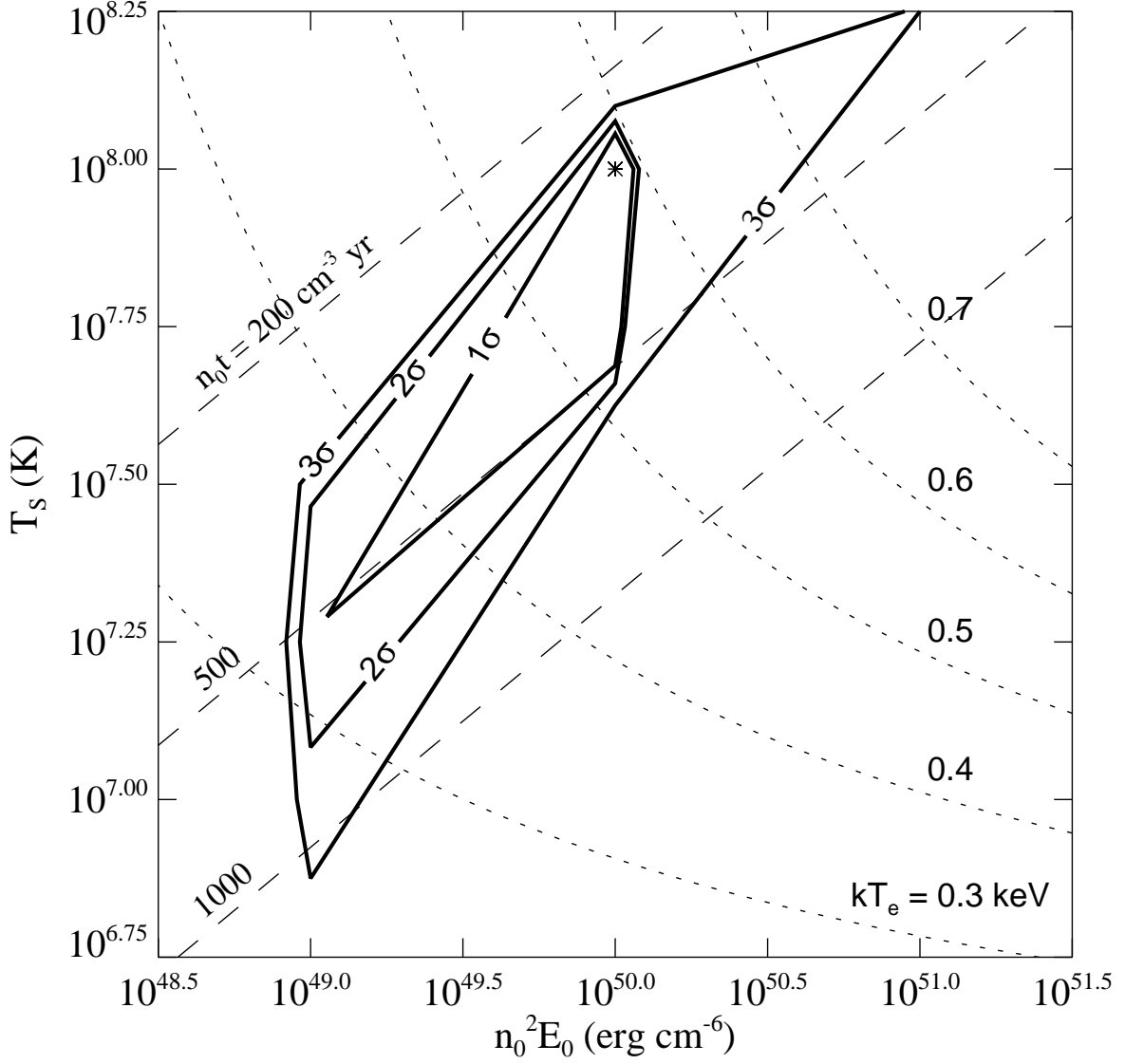


Fig. 5.— 1, 2, and 3 σ confidence level contours for the plane of parameter space defined by two of the parameters of the nonequilibrium ionization thermal component. Here T_s is the temperature associated with the forward shock and $n_0^2 E_0$ is the product of the square of the ambient density of hydrogen and the initial kinetic energy of the ejecta. The best-fit values of these parameters are indicated by the asterisk. From top to bottom, the three dashed lines are lines along which the ionization timescale $n_0 t = 200, 500$, and $1000 \text{ cm}^{-3} \text{ yr}$, respectively. From bottom to top, the five dotted curves are curves along which the characteristic electron temperature $kT_e = 0.3, 0.4, 0.5, 0.6$, and 0.7 keV , respectively.

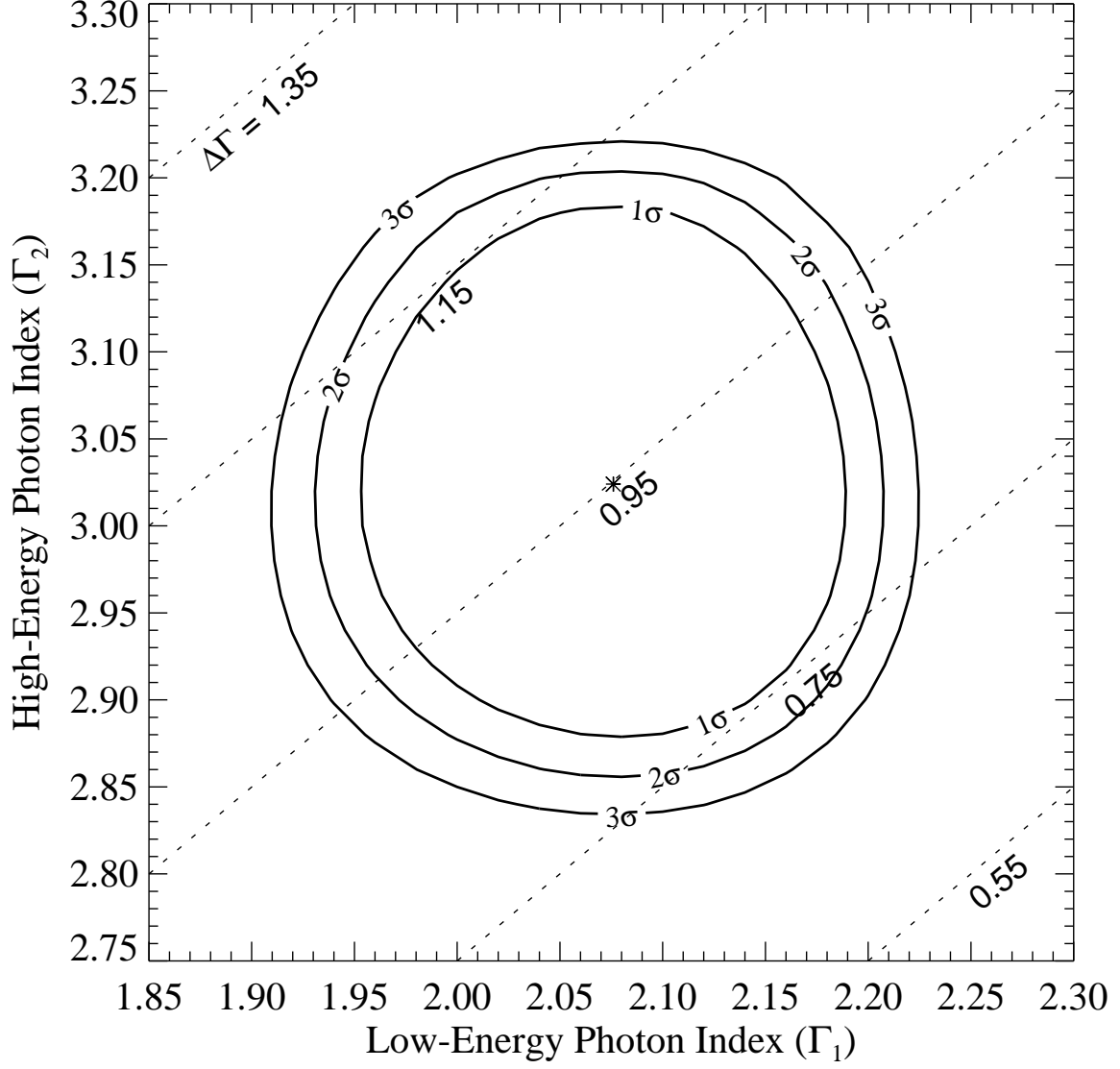


Fig. 6.— 1, 2, and 3 σ confidence level contours for the plane of parameter space defined by the photon indices of the broken power law. The best-fit values of the two indices are indicated by the asterisk. The dotted lines are lines along which the difference between the two indices $\Delta\Gamma = \Gamma_2 - \Gamma_1 = 0.55, 0.75, 0.95, 1.15$, and 1.35 . The nonthermal X-ray spectrum of SN 1006 steepens with increasing energy since the line defined by $\Delta\Gamma = 0$ is excluded at much more than the 3 σ confidence level. This result supports the claim that the nonthermal X-ray emission is synchrotron radiation.

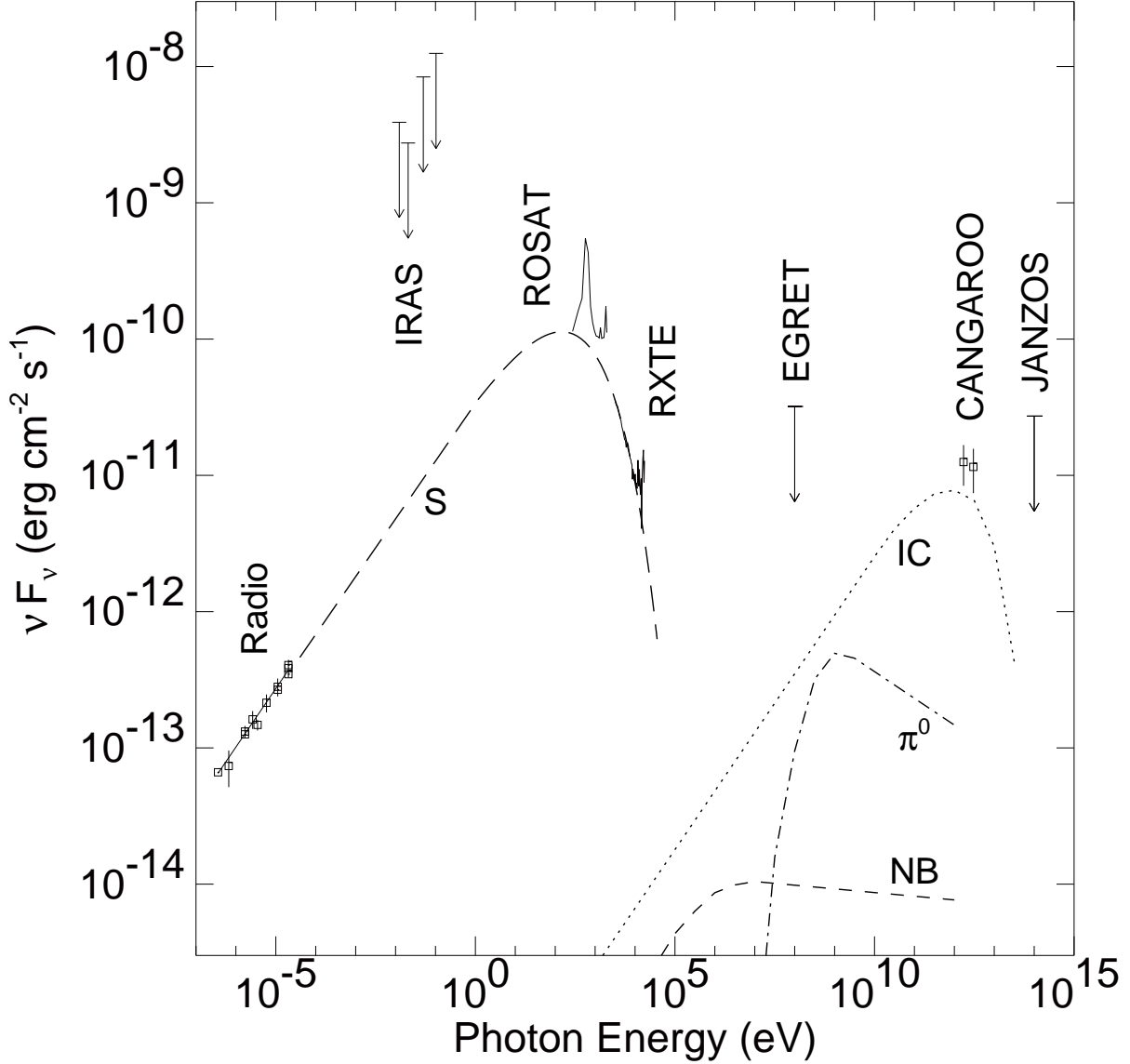


Fig. 7.— Radio to gamma-ray photon energy-flux spectrum of SN 1006. The data, which are labeled vertically, include the radio results of Kundu (1970), Milne (1971), Milne & Dickel (1975), Stephenson, Clark, & Crawford (1977), and Roger et al. (1988), the *IRAS* infrared upper limits of Arendt (1989), the *ROSAT* PSPC and *RXTE* PCA results of this paper, the EGRET gamma-ray upper limit of Hartman et al. (1999, Fig. 3), the gamma-ray results of the CANGAROO collaboration (Tanimori et al. 1998), and the gamma-ray upper limit of the JANZOS collaboration (Allen et al. 1995). The four model spectra are estimates of the photon energy fluxes produced by synchrotron radiation (S), inverse Compton scattering on the cosmic microwave background radiation (IC), the decay of neutral pions (π^0), and bremsstrahlung emission of the nonthermal

electrons (NB). The nonthermal X-ray spectrum is consistent with a model of the synchrotron spectrum, but the data are not consistent with the models of nonthermal bremsstrahlung and inverse Compton scattering.

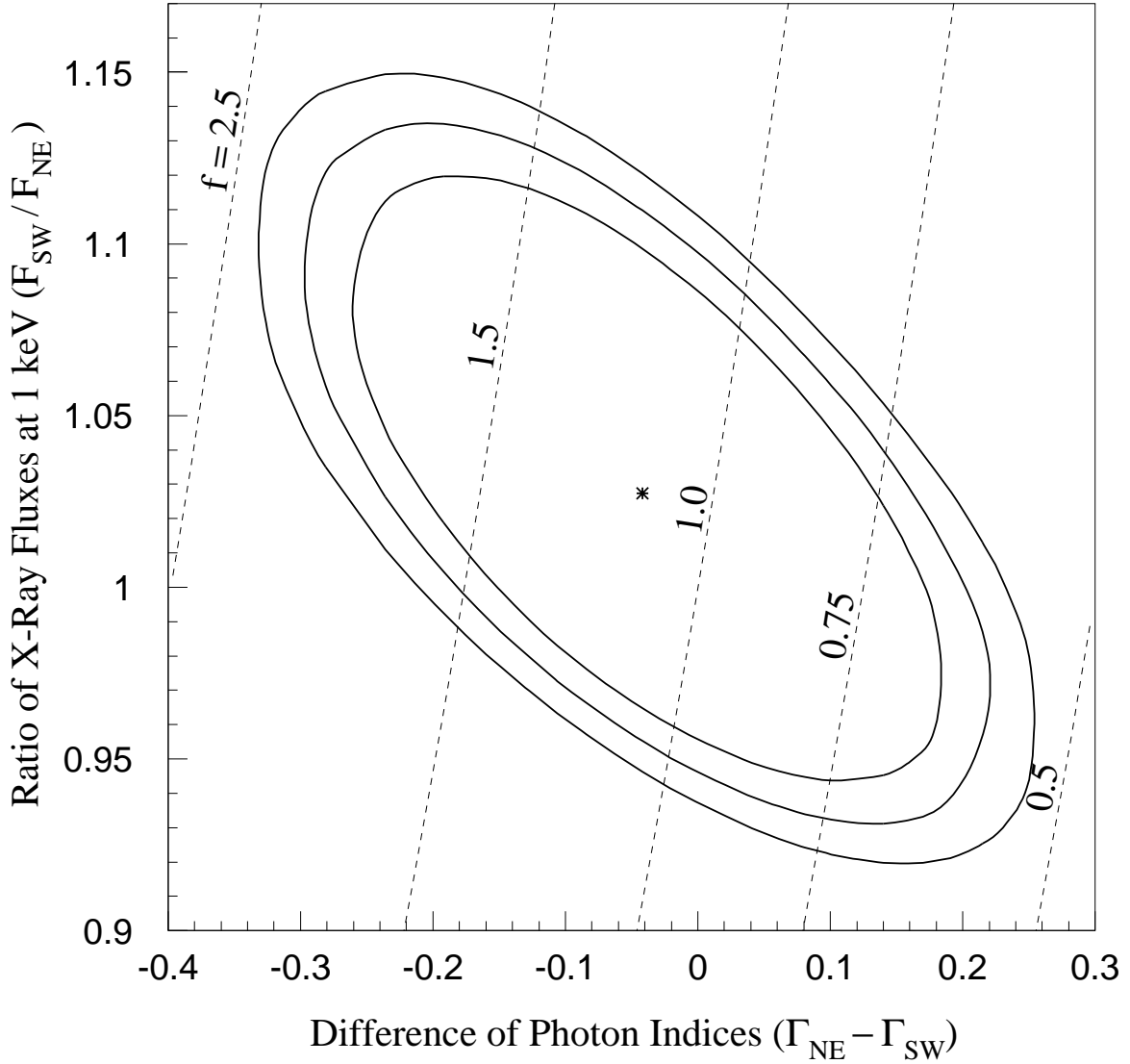


Fig. 8.— Comparison of the nonthermal X-ray spectra of the northeastern and southwestern rims of SN 1006 in the *ROSAT* PSPC energy band. Here $\Gamma_{\text{NE}} - \Gamma_{\text{SW}}$ is the difference between the photon indices of the two rims and $F_{\text{SW}}/F_{\text{NE}}$ is the ratio of the nonthermal fluxes at 1 keV. The best-fit values of the two parameters are indicated by the asterisk. The low-energy nonthermal spectra of the two rims are consistent with each other because the point defined by $\Gamma_{\text{NE}} - \Gamma_{\text{SW}} = 0$ and $F_{\text{SW}}/F_{\text{NE}} = 1$ is inside the 1σ confidence level contour. From the right to the left, the five dashed curves are curves along which $F_{\text{SW}}/F_{\text{NE}} = 0.5, 0.75, 1, 1.5$, and 2.5 , respectively, at 0.1 keV.

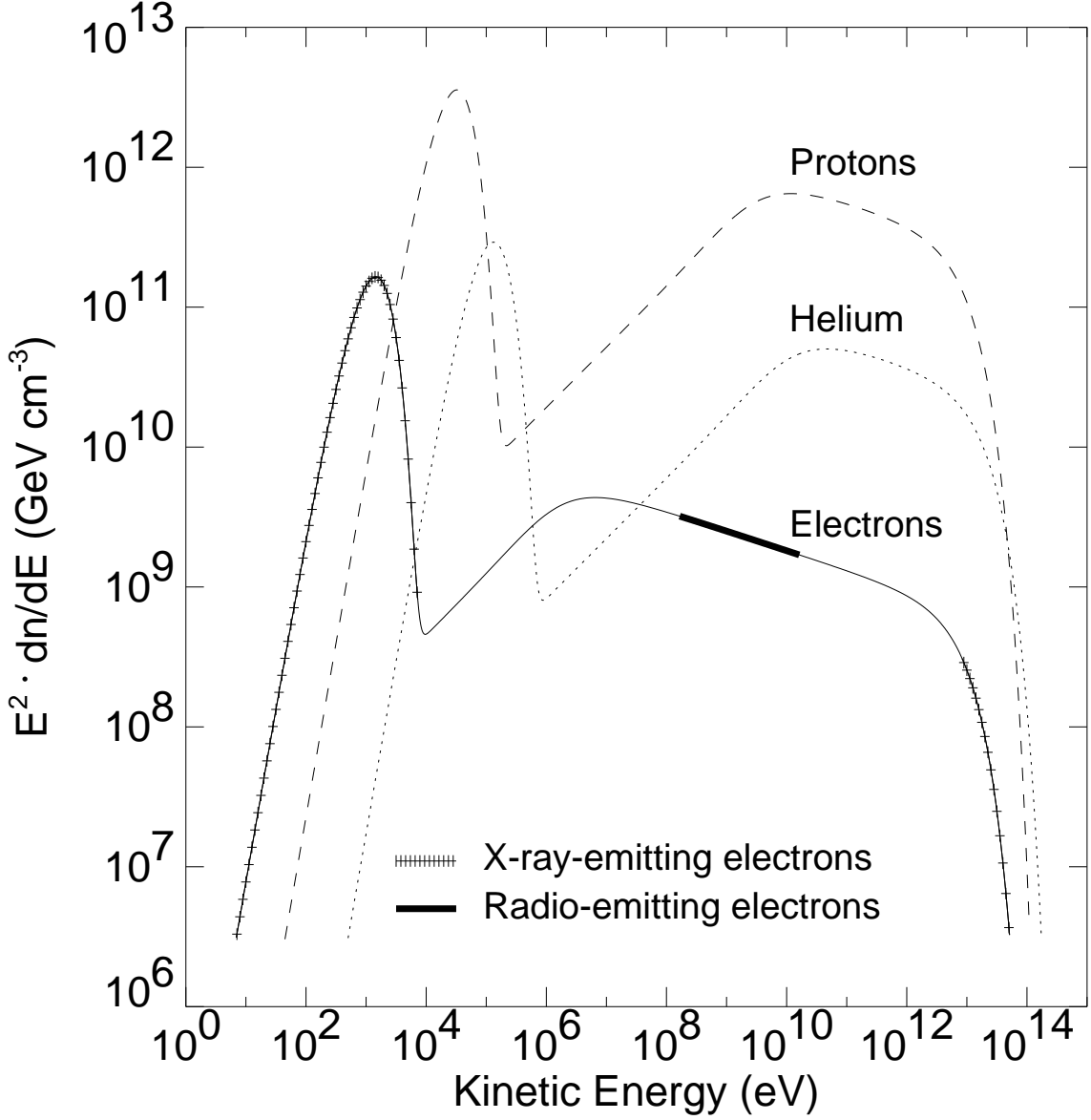


Fig. 9.— Estimates of the cosmic-ray electron, proton, and helium spectra of SN 1006. The low- and high-energy ends of the electron spectrum produce the observed thermal and nonthermal X-ray emission, respectively. The GeV electrons produce the observed radio emission. The ratio of the number densities of protons and electrons at 1 GeV is about 160, which is consistent with the ratio observed at Earth. The total cosmic-ray energy is dominated by the energy of the cosmic-ray protons.

Table 1. Results Obtained Using Two-Component Models

Model ^a	n_{H} (10^{20} atoms cm^{-2})	Component 1 (Dimensionless or keV)	Component 2 (keV or cm^{-3} s)	χ^2/ν
BPL+NEI	$5.60^{+0.58}_{-0.51}$	$\Gamma_1 = 2.08^{+0.11}_{-0.13}$ $E_b = 1.85^{+0.18}_{-0.16}$ $\Gamma_2 = 3.02^{+0.16}_{-0.14}$	$kT_e = 0.58^{+0.01}_{-0.24}$ $n_0t = 8.6^{+7.7}_{-0.7} \times 10^9$	1109/729
BPL+RS	$5.83^{+0.71}_{-0.60}$	$\Gamma_1 = 2.06^{+0.11}_{-0.12}$ $E_b = 1.90^{+0.15}_{-0.12}$ $\Gamma_2 = 3.14^{+0.08}_{-0.09}$	$kT_e = 0.162^{+0.009}_{-0.009}$	1202/729
PL+NEI	$6.48^{+0.52}_{-0.44}$	$\Gamma = 2.51^{+0.04}_{-0.05}$	$kT_e = 0.58^{\text{b}}$ $n_0t = 8.6 \times 10^9^{\text{b}}$	1864/731
Brem+NEI	$5.13^{+0.65}_{-0.57}$	$kT_{e1} = 2.19^{+0.09}_{-0.10}$	$kT_{e2} = 0.58^{\text{b}}$ $n_0t = 8.6 \times 10^9^{\text{b}}$	2338/731

^aThese X-ray spectral models include a power law (PL), a broken power law (BPL), a thermal bremsstrahlung model (Brem), a thermal model based on the work of Raymond & Smith (1977; RS), or a nonequilibrium ionization model (NEI; Hamilton et al. 1983).

^bThe 1σ errors of the characteristic electron temperatures, kT_e , and the ionization time-scales, n_0t , of the NEI model were not determined for these two sets of models, but they are expected to be similar to the uncertainties listed for the BPL+NEI model.

Table 2. Parameters of the Best-Fit Model^a

Parameter	Value	90% Interval ^b
Interstellar absorption component		
n_{H} (10^{20} atoms cm^{-2})	5.60	5.04–6.24
Broken power law component ^c		
Γ_1	2.08	1.94–2.20
E_b (keV)	1.85	1.66–2.05
Γ_2	3.02	2.86–3.19
Flux(0.1–2 keV) (10^{-10} erg cm^{-2} s^{-1})	1.42	1.31–1.54
Nonequilibrium ionization component		
T_{is} (K)	10^8	$10^{7.25-10^8}$
$n_0^2 E_0$ (ergs cm^{-6})	10^{50}	$10^{49-10^{50}}$
He ^d	1	...
C ^d	1	...
N ^d	1	...
O	1.6	0.8–2.8
Ne	0.3	0–0.8
Mg	2.0	0–5.9
Si ^e	16	10–18
S ^e	16	10–18
Ca ^e	16	10–18
Fe ^d	1	...
Ni ^d	1	...
Flux(0.1–2 keV) (10^{-10} erg cm^{-2} s^{-1})	2.53	2.25–2.91

^aThis model is the “BPL+NEI” model of Table 1.

^bThe 90% confidence level intervals are computed using only the statistical uncertainties.

^c $dF/dE = K(E/1 \text{ keV})^{-\Gamma_1}$ for $E < E_b$ and $dF/dE = K(E_b/1 \text{ keV})^{\Gamma_2-\Gamma_1}(E/1 \text{ keV})^{-\Gamma_2}$ for $E \geq E_b$.

^dThe relative abundances of the elements helium, carbon, nitrogen, iron, and nickel are fixed to be the same as the relative solar abundances (Anders & Grevesse 1989) of these elements.

^eThe relative abundances of the elements sulphur and calcium are fixed to be the same as the relative abundance of silicon.

Table 3. Parameters Inferred from the Best-Fit Thermal Model

Parameter	Value	90% Interval ^a
kT_e (keV)	0.58	0.31–0.60
v_{fs} (km s ^{−1})	2700	1000–2900
r_{fs} (pc)	5.9 ^b	5.6–16.3
d ($= r_{\text{fs}}/\theta$) (kpc)	1.4 ^{b,c}	1.3–3.7
$n_0 t$ (10 ⁹ cm ^{−3} s)	8.6	7.6–20.6
t (yr)	870 ^b	760–6300
n_0 ($= (n_0^2 E_0/E_0)^{1/2}$) (cm ^{−3})	0.32 ^b	0.10–0.37
E_0 (10 ⁵¹ ergs)	1.00 ^b	...
M_s (M_\odot)	9.7 ^b	8.3–67

^aThe 90% confidence level intervals are computed using only the statistical uncertainties.

^bThese parameters depend on E_0 , which is assumed to be 10⁵¹ ergs. The parameters r_{fs} , d , and t scale as $(E_0/10^{51} \text{ ergs})^{1/2}$. The parameter n_0 scales as $(E_0/10^{51} \text{ ergs})^{-1/2}$. The parameter M_s scales as $(E_0/10^{51} \text{ ergs})$.

^cThe angular radius $\theta = 15'$.

Table 4. Inferred Distribution of Energy

Parameter	Value (ergs)
$E_{\text{kin}} = \frac{1}{2} M v^2 \approx \frac{9}{32} M_s v_{\text{fs}}^2$	$4 \times 10^{50 \text{a}, \text{b}}$
$E_{kT_p} = \frac{3}{2} N_p k T_p \approx \frac{3}{8} \pi m_p n_0 r_{\text{fs}}^3 v_{\text{fs}}^2$	$4 \times 10^{50 \text{b}}$
$E_{kT_e} = \frac{3}{2} N_e k T_e \approx 2 \pi \frac{n_e}{n_p} n_0 r_{\text{fs}}^3 k T_e$	$2 \times 10^{49 \text{b}}$
E_B	$3 \times 10^{47 \text{c}}$
E_{cr}	$1 \times 10^{50 \text{d}}$
Distribution of cosmic-ray energy $E_{\text{cr}}^{\text{c}, \text{d}}$	
E_e	9×10^{47}
E_p	1×10^{50}
E_{He}	8×10^{48}

^aThe kinetic energy of the unshocked ejecta is neglected.

^bThese parameters scale as $(E_0/10^{51} \text{ ergs})$.

^cThe magnetic field strength in SN 1006 is assumed to be $40 \mu\text{G}$.

^dWithin an accuracy of about 25%, these parameters scale as $(B/40 \mu\text{G})^{-1}$.

Table 5. Parameters of the Cosmic-Ray Spectra

Particle	A ($\text{cm}^{-3} \text{ GeV}^{\Gamma-1}$)	Γ	ϵ (TeV)
Electrons	2.4×10^{-9}	2.14 ± 0.12	10
Protons	1.1×10^{-6}	2.14	10
Helium	1.0×10^{-7}	2.14	20

Note.—The cosmic-ray injection efficiency $\eta = 5 \times 10^{-4}$ and is assumed to be independent of the particle species (see sec. 4.3). The ratio of the number density of cosmic-ray protons to the number density of cosmic-ray electrons is 160 at 1 GeV (Fig. 9).